Accepted Manuscript

Disorder-to-helix conformational conversion of the human immunomodulatory peptide LL-37 induced by antiinflammatory drugs, food dyes and some metabolites

Ferenc Zsila, Gergely Kohut, Tamás Beke-Somfai

PII: S0141-8130(18)37006-5
DOI: https://doi.org/10.1016/j.ijbiomac.2019.01.209
Reference: BIOMAC 11642

To appear in: *International Journal of Biological Macromolecules*

Received date: 15 December 2018
Revised date: 29 January 2019
Accepted date: 31 January 2019

Please cite this article as: F. Zsila, G. Kohut and T. Beke-Somfai, Disorder-to-helix conformational conversion of the human immunomodulatory peptide LL-37 induced by antiinflammatory drugs, food dyes and some metabolites, International Journal of Biological Macromolecules, https://doi.org/10.1016/j.ijbiomac.2019.01.209

Disorder-to-helix conformational conversion of the human immunomodulatory peptide LL-37 induced by antiinflammatory drugs, food dyes and some metabolites

Ferenc Zsila*, Gergely Kohut, Tamás Beke-Somfai

Biomolecular Self-Assembly Group, Institute of Materials and Environmental Chemistry, Research Centre for Natural Sciences, Hungarian Academy of Sciences, P.O. Box 286, H-1519, Budapest, Hungary

Corresponding author: Ferenc Zsila

Email: zsila.ferenc@ttk.mta.hu

Abstract

The human antimicrobial and immunomodulatory peptide LL-37 is ubiquitously expressed and secreted by epithelial cells of mucosal surfaces including the gastrointestinal tract, the primary absorption site of orally administered drugs and food components. Besides antimicrobial properties, LL-37 also contributes to the pathophysiology of various diseases such as ulcerative colitis, Crohn's disease and cancer. The non-covalent association of antiinflammatory drugs, porphyrin pigments, bile salts and food dyes to the peptide was uncovered and evaluated by circular dichroism (CD) spectroscopy. These agents induce the disorder-to-order conformational transition of the natively unstructured LL-37 leading to its helical folding. Even in the presence of chloride, where LL-37 is partially folded, these small molecules were able to rise the α-helix content. CD titration data indicated positive cooperativity between the ligand molecules accommodated to the peptide chain resulting in multimeric complexes with apparent dissociation constants ranged from 2 to 500 μM. Computational docking suggested the prominent role of the Lys8–Arg19 segment of LL-37 in the accommodation of ligand molecules, governed principally by salt bridges and H-bonding. Since pleiotropic biological functions of LL-37 are strongly conformation-dependent it could be anticipated that folding inducer compounds may modulate its *in vivo* actions and of related cationic peptides.

Keywords: antiinflammatory drugs; bile acid; circular dichroism; food dyes; helical folding; hemin; intrinsic disorder; LL-37

Abbreviations: CD, circular dichroism

Introduction

Cathelicidins are an important group of animal cationic host defense peptides, the evolutionarily conserved components of the innate immune system [1, 2]. They are also known as antimicrobial peptides, since were originally described on the basis of their direct microbicidal properties. However, growing number of evidences refer to their immunomodulatory capacities that may represent the major biological function. The single human cathelicidin, the 37 amino acids long LL-37, with two N-terminal leucines, is rich in lysine and arginine residues and has +6 net charge under physiological conditions (Scheme 1). Being ubiquitously produced by epithelial cells and phagocytic leukocytes, it can be detected in a variety of tissues and body fluids such as skin, airway surfaces, gastrointestinal/urogenital tract, bone marrow, blood plasma, breast milk, saliva and tear [3, 4]. In addition, the overexpression of LL-37 in some malignant tumors has recently been demonstrated [5]. Besides its broad antimicrobial activities against bacteria, fungi, and viral pathogens [6, 7], LL-37 also exhibits multiple pathophysiological roles including cell proliferation, apoptosis, angiogenesis, tissue repair, chemoattraction, and even carcinogenesis/metastasis [4, 8]. For instance, LL-37 possesses complex and intricate functions in the pathogenesis of Crohn's disease and ulcerative colitis, the immune-mediated chronic inflammatory disorders of the gastrointestinal tract [9-11]. According to the current view, inflammatory bowel diseases are caused by a dysregulated immune response to the intestinal microbiota in genetically susceptible hosts. Since LL-37 is implicated in a variety of disease processes at diverse organ sites, it attracts increasing attention as template for the development of novel immunomodulatory therapeutics [12, 13].

As it has been shown in our previous reports, the secondary structure of cationic AMPs can deeply be altered by various small molecules [14, 15]. Some anionic pharmaceutical agents as well as endogenous metabolites (hemin, bile pigments) were able to induce disorder-to-helix transitions of the bee venom component melittin and its semisynthetic derivative. This structural transformation is analogous to the well-known, membrane binding-induced folding of LL-37 and other AMPs which is triggered by the anionic phospholipid head groups resulting in amphipathic α-helices (Scheme 1) [3, 12, 16]. However, structural rearrangements of LL-37 may be important not only for membrane-directed antimicrobial activity but also for its specific binding to a variety of receptors and consequent receptor-mediated pleiotropic effects on host cells [17, 18]. It was found by 20 years ago, that the secondary structure of LL-37 is highly sensitive to the presence of inorganic anions. Whereas it is unstructured in deionized water, adopts α-helical

conformation upon addition of chloride, phosphate, sulfate or bicarbonate ions used typically at millimolar concentrations [12, 19]. Such a structural conversion was ascribed to the ability of these ions to "salt out" nonpolar residues of the peptide as well as to shield repulsive electrostatic forces between positively charged side chains. Taking these data and our previous observations into consideration, it could be assumed that the conformation of LL-37 can also be altered by acidic organic molecules. To test this hypothesis, circular dichroism (CD) spectroscopy was employed to evaluate the secondary structure of the native peptide in the presence of various xenobiotics and some metabolites of the human body [20-23]. The compounds used can be divided into the following categories: non-steroidal antiinflammatory drugs, antiallergic agents, suramin, TNS, food dyes, endogenous porphyrin derivatives and bile acids (Scheme 2). These pharmaceutical substances are widely employed in the clinical practice to treat a number of disorders, in the pathomechanisms of which LL-37 is involved (*e.g.*, Crohn's disease, ulcerative colitis [24], systemic lupus erythematosus [25], arthritis [26] *etc*.). Synthetic food colors commonly consumed by the human population worldwide are linked to immune-mediated negative behavioral effects in children [27]. Porphyrin pigments and bile salts are continuously produced in the human body and interact with the gut microbiome and epithelial cells which produce LL-37. Similarly to the peptide, bile salts are also associated with the pathogenesis of various gastrointestinal disorders, such as inflammatory bowel diseases and colorectal cancer [28-30]. Furthermore, dietary heme-induced damage and consequent hyperproliferation of the colonic epithelial surface cells have been demonstrated emphasizing the synergistic role of the gut microbiota by reducing the mucus barrier function [31].

Materials and Methods

Materials

Hemin, bilirubin ditaurate and stercobilin HCl (mixture of isomers) were purchased from Frontier Scientific. Balsalazide disodium salt dihydrate, olsalazine sodium, sulfasalazine (all from Santa Cruz Biotechnology), salicylic acid (Sigma-Aldrich), diclofenac sodium salt (Sigma-Aldrich), meclofenamic acid sodium salt (MP Biomedicals), (±)-ibuprofen (Andeno B.V.), cromolyn sodium salt (Sigma-Aldrich), cetirizine 2HCl (AK-Scientific, Inc.), taurocholic acid sodium salt hydrate (Sigma- Aldrich), sodium glycocholate hydrate (Sigma-Aldrich), suramin sodium salt (Calbiochem), allura red AC (Sigma-Aldrich), tartrazine (Sigma-Aldrich) and 2-(*p*-toluidino)-6-naphthalenesulfonic acid potassium salt (TNS, Sigma-Aldrich) were used as supplied. Imatinib (free base) was a gift from the Vichem Chemie Research Ltd. (Budapest, Hungary). All other chemicals were of analytical reagent grade.

Peptide synthesis and characterization

LL-37 amide (cat. no.: 308114, LLGDFFRKSKEKIGKEFKRIVQRIKDFLRNLVPRTES-NH_2) was synthesized by NovoPro Bioscience Inc. (Shanghai, China). Peptide purity corresponded to 96.20%. Molecular mass of the peptide (4492.25) was determined by mass spectrometry. The net peptide content of the supplied material was 72.12% (Shanghai Institute of Organic Chemistry, Chinese Academy of Sciences).

Preparation of peptide and ligand stock solutions

18 μM LL-37 solution was prepared in salt-free or salted (130 mM NaCl) Tris-HCl buffer (10 mM, pH 7.4) which was aliquoted and freezed at -20 °C. Hemin was first dissolved in 0.1 M NaOH and subsequently diluted by salt-free Tris-HCl buffer to obtain 0.5 mM solution. Stock solutions of all other compounds were made by using 10 mM salt-free Tris-HCl buffer (pH 7.4).

Circular dichroism spectroscopic measurements

All CD spectra were measured on a JASCO J-715 spectropolarimeter at 25 ± 0.2 °C in 0.1 cm path-length rectangular quartz cuvette (Hellma, USA). Temperature control was provided by a Peltier thermostat. CD data were collected in continuous scanning mode between 190 and 260 nm at a rate of 50 nm/min, with a step size of 0.1 nm, response time of 4 sec, three accumulations, and 2 nm bandwidth. CD curves of free peptide and ligand-peptide samples were corrected by the spectral contribution of the blank buffer solution. For CD titration measurements, 200 μL LL-37 solution (18 μM) was placed in the cuvette. After finishing the CD scans of the free peptide, μL aliquots of ligand stock solutions were pipetted consecutively into the cuvette and the CD data were collected after each aliquot.

Secondary structure analysis

Deconvolutions of CD spectral sets obtained by titration of LL-37 with various compounds were performed with the Convex Constraint Algorithm Plus (CCA+) developed to extract base spectra representing common secondary structure motifs and their fractional contributions in a set of experimental CD curves [32, 33]. In addition to optimal basis spectra, CCA+ also yields the relative weights of each basis spectrum under all experimental conditions, which are indicative of the relative populations of each state. The analysis was performed using the CCA+ software with default settings and varying only the number of basis spectra. The plot of RMSD (root mean square deviation) versus numbers of basis spectra shows a distinct kink when three spectra were used, indicating this to be a significantly better fit than with two curves (Fig. S1). Using four or more spectra resulted in only a modest fit improvement. CCA+ analysis produced two types of deconvolution results (Fig. S2). Type A: one component represents the α-helix CD contribution and two, slightly different curves are correlated with the random coil (disordered) fraction. Type B: random coil, α-helix and α-helical coiled coil spectrum.

Calculation of ligand-peptide binding parameters

Non-linear curve fitting analysis of the CD titration data as well as the helical contents derived from the CCA+ analysis were performed by using the “One site - specific binding with Hill slope” equation built in the Graph Pad Prism software (ver. 6.01, San Diego, California, USA).

Standard deviations of the apparent K_d values and the Hill coefficients (h) are shown in the corresponding Tables.

Computational details

Structure of LL-37

The helical solution NMR structure of the human LL-37 peptide (PDB entry: 2K6O) was applied as a rigid receptor structure for dockings [34]. Gasteiger charges were added, and the total charge of LL-37 was +6.

Structure and parameters of the ligands

Based on the K_d values obtained from CD spectroscopic measurements and considering the classification of the small molecules, the following ones were selected for docking: olsalazine, balsalazinde, sulfasalazine, diclofenac, meclofenamic acid, ibuprofen, glycocholate, allura red AC, tartrazine, TNS. The ZINC database [35] was used to obtain the 3D structures (olsalazine: ZINC3812865; balsalazide: ZINC3952881; sulfasalazine: ZINC3831490; diclofenac: ZINC1281; meclofenamic acid: ZINC1655; ibuprofen: ZINC2647; glycocholate: ZINC8143774; allura red AC: ZINC100048689; TNS: ZINC2168595). In cases where multiple structures were provided within one database entry, that one which corresponds to pH 7.4 was selected. However, the 3D structure of tartrazine provided by ZINC database (ZINC100048501) differs from that reported in the literature at pH close to physiological conditions [36]. Thus, the structure relevant in these conditions was parameterized applying the same methodology as of molecules presented in ZINC database [37]: the 3D structure was created and optimized using MarvinSketch (ver. 18.13.0, Chemaxon, 2018) and the partial charges was calculated using AMSOL (ver. 7.1, University of Minnesota, Minneapolis, 2004).

Docking procedure

Dockings of the flexible ligands onto the rigid receptor were carried out by Autodock 4.2 [38] applying the following parameters. The box grid size was chosen to contain (127×127×127) grid points with a spacing of 0.497 Å. The number of individuals in the population was set to 300 using a maximum of 105 generations and 9,995 × 10^5 energy evaluations per docking. Further parameters were chosen to be default and the Lamarckian genetic algorithm was applied to carry

out the dockings. The initial position and conformation of the ligand was random and in sum, 1,000 docking/ligand were performed on LL-37.

Clustering

Hierarchical agglomerative clustering (bottom-up) procedure was applied on all ligands, using AmberTools ver. 16 cpptraj package [39]. The finishing criteria of minimum distance between clusters (ε) was set to 5 Å and the number of remaining clusters (n) were chosen to be 5. RMSD of all atoms were used as distance metric without fitting the structures before calculating the RMSD. The three most populated clusters were chosen for further analysis. The structure in each cluster that has the lowest cumulative distance to every other point was considered as a representative.

Molecular surface calculation was carried out on all docking of each ligand using the *cpptraj molsurf* command and the averages were used as representative values.

Results and Discussion

CD spectroscopic evaluation of the impact of small molecules on the secondary structure of LL-37

The far-UV CD spectrum of LL-37 obtained in salt-free Tris-HCl buffer at pH 7.4 is dominated by a negative peak of π-π^* origin centered around 202 nm whereas the n-π^* transitions of the amide chromophores generate a less intense, broad band displaying a minimum at 225 nm (Fig. 1). In line with previous experimental data, this CD signature is characteristic to the unstructured conformation of LL-37 [19, 40]. To study the effect of various small molecules on the secondary structure of the peptide, CD titration experiments were conducted. Stepwise addition of the guest compounds resulted in dramatic spectral changes (Fig. 1). At the very first phase of the titration, the amplitude of the main negative band decreased and its minimum was shifted to about 205 nm. Upon further addition of the ligands, the peak gained intensity and exhibited more red shift (~209 nm). Concomitantly, a positive band was developed in the short-wavelength region showing a λ_{max} around 193-195 nm and the magnitude of the n-π^* CD band above 215 nm enhanced gradually (Fig. 1). In relation to the free-form of LL-37 that adopts an essentially random coil conformation, the transformed CD curves exhibited distinct double minima (~223-226 and ~209 nm), a zero intercept around 201 nm and a single positive maximum below 200 nm (~193 nm). Such a spectral pattern is consistent with those observed for canonical α-helices implying that in a different extent these compounds are able to provoke the disorder-to-helix transition of LL-37. It is to be noted that the titration curves displayed an isodichroic point around 205 nm signifying that the folding occurs via a dynamic equilibrium between the disordered and the helical species. These conclusions are fully consonant with the deconvolution of the CD spectra showing the progressive increase of the α-helix content (Fig. 2). The most effective drugs which produced the greatest helical transformation (~70% or higher) belong to the antiinflammatory group. The monoacid diclofenac/meclofenamic acid and the dicarboxylic olsalazine/balsalazide resulted in similar CD spectroscopic changes both in quanti- and qualitative terms whereas other NSAIDs triggered a weaker (sulfasalazine, ibuprofen) or only a mild (salicylic acid) structural rearrangement. Despite of the presence of acidic functions and aromatic moieties, the antiallergic cromolyn and cetirizine (Scheme 1) showed only a limited helix-inducing ability which points out some structure-folding inducing activity relationships. The food color tartrazine and allura red AC increased abruptly the helix content that reached a

maximum at around 1:1 dye:peptide molar ratio. In this sense, only the antiprotozoal drug suramin was more effective producing a ~70% α-helix fraction at lower ligand loading of the peptide chain (Fig. 2, Fig. 3). In relation to the other compounds tested in this work, the highest number of the acidic (sulfate) groups in suramin may decisively contribute to its superior folding activity. Interestingly, tartrazine and allura red AC have recently been reported to induce amyloid transformation of serum albumins and β-lactoglobulin under acidic condition (pH 3.5). The formation of cross β-sheet structured fibrils were attributed to electrostatic and hydrophobic dye-protein residue interactions [41-43].

Hemin and its water soluble metabolite bilirubin ditaurate also displayed strong structure ordering effect. In contrast, the bilirubin derivative pigment stercobilin formed via enzymatic reduction by intestinal bacteria proved to be a much weaker inducer. Similarly, addition of the bile salt glyco- and taurocholate resulted in appreciable conformational changes only at large molar excess. As amphipathic molecules constituted from hydrophobic and hydrophilic regions, these steroid acids readily form micelles in aqueous solution [44]. In analogy with lipid membranes, the apolar interior of such particles may promote the helical folding of unstructured peptide sequences. However, the lowest critical micelle concentration of these bile salts (~9 mM for glycocholate [45] and 3-5 mM for taurocholate [46]) is much higher than the concentrations at which the folding of LL-37 was detected (<0.4 mM, Fig. 2).

Based on the relative concentrations of the ligands at which the largest helical fraction was obtained, they can be categorized into three groups (Fig. 3). Strong inducers including suramin, food dyes, hemin, bilirubin, olsalazine, etc. display their maximal folding effect below 70 μM. Diclofenac, balsalazide, cromolyn, TNS and stercobilin belong to the medium category with cc. values in the 100-200 μM range. Finally, bile salts and ibuprofen can be classified as weak inducers being most effective above 300 μM. Comparison of these groups shows that similar conformation-ordering effect is associated to chemically diverse molecules, *e.g.* hemin-olsalazine, meclofenamic acid-bilirubin ditaurate. And *vice versa*, structurally related compounds such as stercobilin-hemin, stercobilin-bilirubin ditaurate and diclofenac-meclofenamic acid own considerably different helix-inducing power. Accordingly, it seems that distinct chemical motifs could exert equivalent ordering effects but even relatively small structural modifications may result in a great impairment in the folding efficiency.

It is to be noted that the *N*-arylaminonaphthalene sulfonate derivative TNS also exhibited a significant structure-ordering effect (Fig. S3). This compound and related naphthalene sulfonate

derivatives (ANS, bis-ANS, bis-TNS) are widely employed as non-covalent fluorescent probes for conformational studies of peptides/proteins [47, 48] or the mechanisms and kinetics of amyloid formation [49]. In this respect, the helix-promoting feature of TNS demonstrated herein implies that this molecule (and likely its congeners) may act not only as a passive reporter but can directly change the secondary structure of target sequences rich in cationic residues.

In order to test whether ligand-side chain hydrophobic interactions alone are capable to induce helical folding, the tyrosine kinase inhibitor drug imatinib having multiple aromatic rings but no anionic groups was used. Addition of the drug to LL-37 caused only a moderate intensity reduction of the main CD band and left the n-π^* region unaltered (Fig. S4).

Calculation of ligand-peptide binding parameters

The increase of the α-helical content (%) of LL-37 obtained from the analysis of the CD spectra were plotted against the concentrations of the inducers applied during the titrations. Non-linear regression analysis of these data points yielded the apparent dissociation constant (K_d) and the Hill coefficient (Fig. S3). The values calculated by this way are in a good correlation with those derived from the non-linear regression analysis of the CD extremum of the n-π^* band measured around 223-226 nm (Table 1). According to the *h* values found greater than one for all compounds, there is a positive binding cooperativity between the ligand molecules bound to multiple sites along the peptide chain, *i.e.* accommodation of the first molecule enhances the binding of the second one. Suramin exhibited the greatest binding affinity (2 μM) followed by food colors, bilirubin ditaurate, olsalazine and hemin. NSAIDs and TNS bind to LL-37 less avidly whereas the affinity of ibuprofen, cromolyn and bile salts is lower by an order of magnitude (Table 1).

Effect of chloride on the ligand induced folding of LL-37

Chloride is the major anion in the extracellular fluid compartments including blood plasma and interstitial fluids (95-110 mM). In addition, it is the most significant component of airway surface liquid (120-125 mM) as well as gastric and intestinal juices [50, 51]. As previous experiments demonstrated, addition of chloride or other inorganic anions provoke the disorder-to-helix transition of LL-37 [19]. Therefore, Tris-HCl buffer solution of LL-37 was titrated with NaCl to determine the extent of α-helicity at rising chloride concentrations (Fig. S5). As the sigmoidal shape of the titration curve demonstrates, chloride ions from ~50 mM cooperatively

promote the helical transformation of the peptide resulting in a maximal helical content (~80%) above 300 mM. However, the helix fraction is only ~25-35% around physiological Cl^- levels (100-130 mM). Therefore, the conformational effect of some efficient helix promoters was tested on LL-37 dissolved in 10 mM Tris-HCl buffer solution containing 130 mM sodium chloride. In most instances, addition of the ligands produced intensity increase both of the n-π^* and π-π^* CD bands at 224 and 208 nm, respectively, and the development of a positive CD feature below 200 nm (Fig. 4). These changes associated with the red shift of the π-π^* peak enhance the helical feature of the spectrum suggesting the rise of the helix content and thus the preserved fold-inducing activity of the molecules at a chloride level characteristic to *in vivo* conditions. In relation to the K_d values estimated at 10 mM chloride (Table 1), the LL-37 binding of olsalazine and diclofenac did not change significantly, whereas balsalazide, meclofenamic acid and tartrazine exhibited weaker affinity (Table 2). Using of hemin, bilirubin ditaurate and suramin resulted in the progressive increase of the CD_{222}/CD_{208} ratio indicating the peptide aggregation promoting effect of these agents at higher chloride concentration (Fig. S6).

Computational studies

To reveal potential binding poses and gain a molecular level insight on the atomistic interactions between LL-37 and different classes of molecules, some of them were docked 1,000 times to the helical form LL-37 [34] followed by the clustering of the docked structures. Table 3 shows the molecular properties, binding affinities and clustering results of the selected compounds. The evaluation of the binding free energies indicated positive binding affinity towards LL-37, which is in line with the experimental data. The absolute values of the calculated dissociation constants ($\overline{K}_d^{calc}$) differs in average by one order of magnitude compared to those derived from the spectroscopic experiments, which is expected considering the drawbacks of rigid receptor-flexible ligand docking and the diverse chemical nature of the molecules under study [52, 53]. The relative rankings of the K_d values are in a good coincidence with those obtained experimentally (Fig. 5). The only exception is the antiinflammatory drug ibuprofen, which exhibited opposite ranks compared to the experimental results (see the corresponding Spearman's correlation coefficients in Table S1 and S2). This may be related to the considerably different approaches used to estimate the binding affinities. K_d obtained from CD experiments is associated with the helical folding ability of the ligands which is mediated by dynamic, multimolecular interactions with the peptide chain. In contrast, the calculated binding free

energies stem from the consideration of various physicochemical interactions found between the ligand and the helical peptide. It also needs to be stressed, that the semi-empirical Autodock4 force field was calibrated on ligand-protein complexes [38] instead of the much more flexible peptides, whereas conformational freedom, protonation state and charge distribution of the ligands can potentially affect the docking results [52, 54]. Furthermore, the calculated binding free energies and dissociation constants are the averages of different docking poses as we had no structural information about the preferred binding sites. As a result, the energies and dissociation constants might be correlated with the number of different binding poses (which is represented in our study by the total number of clusters as clustering was applied to differentiate between different docking poses) and the surface area of the molecules; see Table S1).

To reveal the potential binding sites, the docked structures were clustered (see Computational details). The three most populated clusters of each ligand were analyzed (Table 3). In the majority of the cases, the most populated cluster was also energetically the most favoured. Exceptions are the clusters of olsalazine and TNS of which the first cluster showed no significant binding energy difference with at least one of the clusters. In addition, the second cluster of ibuprofen has slightly, but significantly better binding energy with almost same population size. Based on these findings, the representatives of the first cluster of each compound was considered as typical binding site, except for ibuprofen where the representative structure of the second cluster was used as characteristic binding pose. Accordingly, tartrazine (Fig. 6), sulfasalazine (Fig. S7) and balsalazide (Fig. S8) bind preferably to the same, lysine-rich segment of LL-37 which could be a consequence of the structural and charge-related similarities they share. Salt bridges between the negatively charged carboxylate or sulfonate groups and the adjacent basic residues (Lys12, Lys15, Lys10 or Lys18) are characteristic for these compounds. Olsalazine is in a slightly different position, but still occupies the same site, as it binds to Lys10 and Lys18 with its anionic groups (Fig. S9).

Diclofenac, meclofenamic acid and TNS also share similarities with respect to their binding pose: the negatively charged moieties make salt bridges with Lys10, while their aromatic ring is close to the Phe6 residue (Fig. 7, Fig. S10 and S11).

In case of ibuprofen, salt bridges between the carboxylate group and Lys15/Arg19 residues stabilize the binding (Fig. S12). Besides the salt bridge between the carboxyl group and the Lys12, the hydroxyl and amide functions of glychocolate establish four H-bonds with Glu16 and Lys8 (Fig. S13).

The energy- and population-based analysis of the binding sites suggests the importance of electrostatic interactions between negatively charged groups of the compounds and basic residues of LL-37. The results underline the significance of the “lysine core” (Lys8, Lys10, Lys12, Lys15, Lys18) and proximal arginines (Arg7, Arg19), especially when considering other clusters as well (Fig. S14). Therefore, it can be assumed that the peptide folding is mediated by multiple insertion of the anionic ligand molecules among the adjacent cationic side chains decreasing the repulsive ionic forces between them and thus allowing helix formation (Fig. 8). This mechanism is especially favoured for ligands owing negative charge at both ends such as suramin, tartrazine, olsalazine, etc. (Scheme 2).

Conclusions

The CD spectroscopic data presented herein unveil the pronounced impact of a chemically diverse set of small molecules on the secondary structure of LL-37. Governed by electrostatic and hydrophobic ligand-side chain interactions, these agents induce disorder-to-helix conformational transition or significantly increase the helical content of the peptide folded partially at physiological chloride concentration. Results from docking of selected compounds to the helical structure of LL-37 gave useful information about molecular details of the binding and provide a potential structural explanation of the fold-inducing effect of antiinflammatory drugs and food dyes. Despite of well-known boundaries, molecular docking methods are potentially susceptible to screen fold-inducing ability of additional molecules on LL-37 and other antimicrobial peptides. Since the mechanism of action of LL-37 is strongly conformation-dependent, our results suggest that these folding inducers may affect the biological activities of the peptide. Food dyes as well as antiinflammatory drugs used routinely in the clinical practice may perturb LL-37 mediated pathways especially in the gastrointestinal tract with currently unknown outcomes. Similarly, certain metabolic products including hemin, bile pigments and bile salts may act as the endogenous regulators of LL-37 both under normal and pathological conditions. These findings also envisage the general possibility of structural impact of anionic small molecules on disordered peptide/protein sequences enriched in cationic residues. It is hoped that these results will help to understand better the pharmacological effects of drugs as well as the regulatory roles of metabolites and propel the development of novel therapeutics for devastating infectious, inflammatory and malignant disorders.

Acknowledgements

The support of the Momentum programme of the Hungarian Academy of Sciences (LP2016-2), the National Competitiveness and Excellence Program (NVKP_16-1-2016-0007) and the BIONANO_GINOP-2.3.2-15-2016-00017b project is acknowledged.

References

[1] R.M. van Harten, E. van Woudenbergh, A. van Dijk, H.P. Haagsman, Cathelicidins: immunomodulatory antimicrobials, Vaccines (Basel) 6 (2018).

[2] J.H. Wong, X.J. Ye, T.B. Ng, Cathelicidins: peptides with antimicrobial, immunomodulatory, anti-Inflammatory, angiogenic, anticancer and procancer activities, Curr. Protein Pept. Sci. 14 (2013) 504-514.

[3] U.H.N. Durr, U.S. Sudheendra, A. Ramamoorthy, LL-37, the only human member of the cathelicidin family of antimicrobial peptides, Biochim. Biophys. Acta 1758 (2006) 1408-1425.

[4] D. Vandamme, B. Landuyt, W. Luyten, L. Schoofs, A comprehensive summary of LL-37, the factotum human cathelicidin peptide, Cell. Immunol. 280 (2012) 22-35.

[5] X. Chen, X.Q. Zou, G.Y. Qi, Y. Tang, Y. Guo, J. Si, L.H. Liang, Roles and mechanisms of human cathelicidin LL-37 in cancer, Cell. Physiol. Biochem. 47 (2018) 1060-1073.

[6] K.J. Barns, J.C. Weisshaar, Real-time attack of LL-37 on single *Bacillus subtilis* cells, Biochim. Biophys. Acta 1828 (2013) 1511-1520.

[7] P.G. Barlow, E.G. Findlay, S.M. Currie, D.J. Davidson, Antiviral potential of cathelicidins, Future Microbiol. 9 (2014) 55-73.

[8] E. Piktel, K. Niemirowicz, U. Wnorowska, M. Watek, T. Wollny, K. Gluszek, S. Gozdz, I. Levental, R. Bucki, The role of cathelicidin LL-37 in cancer development, Arch. Immunol. Ther. Exp. (Warsz) 64 (2016) 33-46.

[9] J.B. McPhee, C.L. Small, S.A. Reid-Yu, J.R. Brannon, H. Le Moual, B.K. Coombes, Host defense peptide resistance contributes to colonization and maximal intestinal pathology by Crohn's disease-associated adherent-invasive *Escherichia coli*, Infect. Immun. 82 (2014) 3383-3393.

[10] S. Kusaka, A. Nishida, K. Takahashi, S. Bamba, H. Yasui, M. Kawahara, O. Inatomi, M. Sugimoto, A. Andoh, Expression of human cathelicidin peptide LL-37 in inflammatory bowel disease, Clin. Exp. Immunol. 191 (2018) 96-106.

[11] D.H.N. Tran, J.N. Wang, C. Ha, W. Ho, S.A. Mattai, A. Oikonomopoulos, G. Weiss, P. Lacey, M. Cheng, C. Shieh, C.C. Mussatto, S. Ho, D. Hommes, H.W. Koon, Circulating cathelicidin levels correlate with mucosal disease activity in ulcerative colitis, risk of intestinal

stricture in Crohn's disease, and clinical prognosis in inflammatory bowel disease, BMC Gastroenterol. 17 (2017).

[12] D. Xhindoli, S. Pacor, M. Benincasa, M. Scocchi, R. Gennaro, A. Tossi, The human cathelicidin LL-37 - A pore-forming antibacterial peptide and host-cell modulator, Biochim. Biophys. Acta 1858 (2016) 546-566.

[13] K. Kuroda, K. Okumura, H. Isogai, E. Isogai, The human cathelicidin antimicrobial peptide LL-37 and mimics are potential anticancer drugs, Front. Oncol. 5 (2015).

[14] F. Zsila, S. Bősze, K. Horváti, I.C. Szigyártó, T. Beke-Somfai, Drug and dye binding induced folding of the intrinsically disordered antimicrobial peptide CM15, RSC Adv. 7 (2017) 41091-41097.

[15] F. Zsila, T. Juhász, S. Bősze, K. Horváti, T. Beke-Somfai, Hemin and bile pigments are the secondary structure regulators of intrinsically disordered antimicrobial peptides, Chirality 30 (2018) 195-205.

[16] K. Zeth, E. Sancho-Vaello, The human antimicrobial peptides dermcidin and LL-37 show novel distinct pathways in membrane interactions, Front. Chem. 5 (2017).

[17] E.T. Verjans, S. Zels, W. Luyten, B. Landuyt, L. Schoofs, Molecular mechanisms of LL-37-induced receptor activation: An overview, Peptides 85 (2016) 16-26.

[18] X.W. Zhang, G. Bajic, G.R. Andersen, S.H. Christiansen, T. Vorup-Jensen, The cationic peptide LL-37 binds Mac-1 (CD11b/CD18) with a low dissociation rate and promotes phagocytosis, Biochim. Biophys. Acta 1864 (2016) 471-478.

[19] J. Johansson, G.H. Gudmundsson, M.E. Rottenberg, K.D. Berndt, B. Agerberth, Conformation-dependent antibacterial activity of the naturally occurring human peptide LL-37, J. Biol. Chem. 273 (1998) 3718-3724.

[20] P. Alam, S.K. Chaturvedi, T. Anwar, M.K. Siddiqi, M.R. Ajmal, G. Badr, M.H. Mahmoud, R.H. Khan, Biophysical and molecular docking insight into the interaction of cytosine β-D arabinofuranoside with human serum albumin, J. Lumin. 164 (2015) 123-130.

[21] P. Alam, G. Rabbani, G. Badr, B.M. Badr, R.H. Khan, The surfactant-induced conformational and activity alterations in *Rhizopus niveus* lipase, Cell Biochem. Biophys. 71 (2015) 1199-1206.

[22] B. Ahmad, G. Muteeb, P. Alam, A. Varshney, N. Zaidi, M. Ishtikhar, G. Badr, M.H. Mahmoud, R.H. Khan, Thermal induced unfolding of human serum albumin isomers: Assigning residual α helices to domain II, Int. J. Biol. Macromol. 75 (2015) 447-452.

[23] P. Alam, A.S. Abdelhameed, R.K. Rajpoot, R.H. Khan, Interplay of multiple interaction forces: Binding of tyrosine kinase inhibitor nintedanib with human serum albumin, J. Photochem. Photobiol. B 157 (2016) 70-76.

[24] I. Sonu, M.V. Lin, W. Blonski, G.R. Lichtenstein, Clinical pharmacology of 5-ASA compounds in inflammatory bowel disease, Gastroenterol. Clin. North Am. 39 (2010) 559-+.

[25] A.A. Horizon, D.J. Wallace, Risk:benefit ratio of nonsteroidal anti-inflammatory drugs in systemic lupus erythematosus, Expert Opin. Drug Saf. 3 (2004) 273-278.

[26] T.N.C.C.f.C. Conditions, Rheumatoid Arthritis. National clinical guideline for management

and treatment in adults, Royal College of Physicians (UK)

Copyright (c) 2009 Royal College of Physicians of London., London, 2018.

[27] P. Amchova, H. Kotolova, J. Ruda-Kucerova, Health safety issues of synthetic food colorants, Regul. Toxicol. Pharm. 73 (2015) 914-922.

[28] P. Hegyi, J. Maleth, J.R. Walters, A.F. Hofmann, S.J. Keely, Guts and gall: bile acids in regulation of intestinal epithelial function in health and disease, Physiol. Rev. 98 (2018) 1983-2023.

[29] E. Tiratterra, P. Franco, E. Porru, K.H. Katsanos, D.K. Christodoulou, G. Roda, Role of bile acids in inflammatory bowel disease, Ann. Gastroenterol. 31 (2018) 266-272.

[30] E. D'Aldebert, M.J.B.B. Mve, M. Mergey, D. Wendum, D. Firrincieli, A. Coilly, L. Fouassier, C. Corpechot, R. Poupon, C. Housset, N. Chignard, Bile salts control the antimicrobial peptide cathelicidin through nuclear receptors in the human biliary epithelium, Gastroenterology 136 (2009) 1435-1443.

[31] N. Ijssennagger, C. Belzer, G.J. Hooiveld, J. Dekker, S.W.C. van Mil, M. Muller, M. Kleerebezem, R. van der Meer, Gut microbiota facilitates dietary heme-induced epithelial hyperproliferation by opening the mucus barrier in colon, Proc. Natl. Acad. Sci. USA 112 (2015) 10038-10043.

[32] A. Perczel, M. Hollósi, G. Tusnády, G.D. Fasman, Convex constraint analysis: a natural deconvolution of circular dichroism curves of proteins, Protein Eng. 4 (1991) 669-679.

[33] K. Park, A. Perczel, G.D. Fasman, Differentiation between transmembrane helices and peripheral helices by the deconvolution of circular dichroism spectra of membrane proteins, Protein Sci. 1 (1992) 1032-1049.

[34] G.S. Wang, Structures of human host defense cathelicidin LL-37 and its smallest antimicrobial peptide KR-12 in lipid micelles, J. Biol. Chem. 283 (2008) 32637-32643.

[35] T. Sterling, J.J. Irwin, ZINC 15 - Ligand discovery for everyone, J. Chem. Inf. Model. 55 (2015) 2324-2337.

[36] E.P. Mazzola, S.J. Bell, S.A. Turujman, J.N. Barrows, J.E. Bailey, J.B. McMahon, T.K. Germann, W.F. Reynolds, Nuclear magnetic resonance investigations of azo-hydrazone, acid-base equilibria of FD&C Yellow No. 5 (tartrazine), Can. J. Chem. 77 (1999) 1941-1945.

[37] B.Q.Q. Wei, W.A. Baase, L.H. Weaver, B.W. Matthews, B.K. Shoichet, A model binding site for testing scoring functions in molecular docking, J. Mol. Biol. 322 (2002) 339-355.

[38] G.M. Morris, R. Huey, W. Lindstrom, M.F. Sanner, R.K. Belew, D.S. Goodsell, A.J. Olson, AutoDock4 and AutoDockTools4: Automated docking with selective receptor flexibility, J. Comput. Chem. 30 (2009) 2785-2791.

[39] R. Salomon-Ferrer, D.A. Case, R.C. Walker, An overview of the Amber biomolecular simulation package, Wires Comput. Mol. Sci. 3 (2013) 198-210.

[40] D. Xhindoli, S. Pacor, F. Guida, N. Antcheva, A. Tossi, Native oligomerization determines the mode of action and biological activities of human cathelicidin LL-37, Biochem. J. 457 (2014) 263-275.

[41] N.A. Al-Shabb, J.M. Khan, M.A. Alsenaidy, A.M. Alsenaidy, M.S. Khan, F.M. Husain, M.R. Khan, M. Naseem, P. Sen, P. Alam, R.H. Khan, Unveiling the stimulatory effects of tartrazine on human and bovine serum albumin fibrillogenesis: Spectroscopic and microscopic study, Spectrochim. Acta A 191 (2018) 116-124.

[42] N.A. Al-Shabib, J.M. Khan, A. Malik, A.M. Alsenaidy, M.A. Alsenaidy, F.M. Husain, M.B. Shamsi, S. Hidayathulla, R.H. Khan, Negatively charged food additive dye "Allura Red" rapidly induces SDS-soluble amyloid fibril in β-lactoglobulin protein, Int. J. Biol. Macromol. 107 (2018) 1706-1716.

[43] J.M. Khan, M.R. Khan, P. Sen, A. Malik, M. Irfan, R.H. Khan, An intermittent amyloid phase found in gemini (G5 and G6) surfactant induced β-sheet to α-helix transition in concanavalin A protein, J. Mol. Liq. 269 (2018) 796-804.

[44] A.F. Hofmann, L.R. Hagey, Key discoveries in bile acid chemistry and biology and their clinical applications: history of the last eight decades, J. Lipid. Res. 55 (2014) 1553-1595.

[45] S. Reis, C.G. Moutinho, C. Matos, B. de Castro, P. Gameiro, J.L.F.C. Lima, Noninvasive methods to determine the critical micelle concentration of some bile acid salts, Anal. Biochem. 334 (2004) 117-126.

[46] S.M. Meyerhoffer, L.B. Mcgown, Critical micelle concentration behavior of sodium taurocholate in water, Langmuir 6 (1990) 187-191.

[47] C.C. Condie, S.C. Quay, Conformational studies of aqueous melittin. Characteristics of a fluorescent probe binding site, J. Biol. Chem. 258 (1983) 8231-8234.

[48] M. Golczak, A. Kirilenko, J. Bandorowicz-Pikula, S. Pikula, Conformational states of annexin VI in solution induced by acidic pH, FEBS Lett. 496 (2001) 49-54.

[49] M.S. Celej, E.A. Jares-Erijman, T.M. Jovin, Fluorescent *N*-arylaminonaphthalene sulfonate probes for amyloid aggregation of α-synuclein, Biophys. J. 94 (2008) 4867-4879.

[50] M. Gilanyi, C. Ikrenyi, J. Fekete, K. Ikrenyi, A.G.B. Kovach, Ion concentrations in subcutaneous interstitial fluid: measured versus expected values, Am. J. Physiol. 255 (1988) F513-F519.

[51] Y.L. Song, J. Thiagarajah, A.S. Verkman, Sodium and chloride concentrations, pH, and depth of airway surface liquid in distal airways, J. Gen. Physiol. 122 (2003) 511-519.

[52] P. Ferrara, H. Gohlke, D.J. Price, G. Klebe, C.L. Brooks, Assessing scoring functions for protein-ligand interactions, J. Med. Chem. 47 (2004) 3032-3047.

[53] S.F. Sousa, P.A. Fernandes, M.J. Ramos, Protein-ligand docking: Current status and future challenges, Proteins 65 (2006) 15-26.

[54] J.C. Wang, J.H. Lin, C.M. Chen, A.L. Perryman, A.J. Olson, Robust scoring functions for protein-ligand interactions with quantum chemical charge models, J. Chem. Inf. Model. 51 (2011) 2528-2537.

Ligand	K_d (μM)	h	R^2
Hemin	20.0 (±1.5)[h] 36.3 (±3.3)[*]	1.8 (±0.2)[h] 1.5 (±0.1)[*]	0.9954[h] 0.9971[*]
Bilirubin ditaurate	11.4 (±0.8)[h] 18.4 (±1.8)[*]	1.7 (±0.1)[h] 1.7 (±0.2)[*]	0.9990[h] 0.9969[*]
Stercobilin	135 (±13)[h] –	2.0 (±0.2)[h] –	0.9974[h] –
Suramin	2.0 (±0.1)[h] 4.9 (±0.5)[*]	3.1 (±0.2)[h] 1.8 (±0.1)[*]	0.9984[h] 0.9971[*]
Olsalazine	16.2 (±0.5)[h] 16.2 (±0.5)[*]	2.3 (±0.1)[h] 1.9 (±0.1)[*]	0.9976[h] 0.9984[*]
Balsalazide	52.6 (±0.8)[h] 54.1 (±0.7)[*]	2.6 (±0.1)[h] 2.6 (±0.1)[*]	0.9990[h] 0.9993[*]
Sulfasalazine	46.6 (±5.9)[h] 57.5 (±2.8)[*]	1.9 (±0.2)[h] 2.5 (±0.2)[*]	0.9964[h] 0.9973[*]
Diclofenac	83.0 (±4.7)[h] 86.2 (±2.8)[*]	2.4 (±0.2)[h] 2.4 (±0.1)[*]	0.9909[h] 0.9961[*]
Meclofenamic acid	39.2 (±1.5)[h] 48.5 (±1.8)[*]	3.8 (±0.3)[h] 2.6 (±0.2)[*]	0.9955[h] 0.9972[*]
(±)-Ibuprofen	485 (±48)[h] 476 (±51)[*]	2.0 (±0.1)[h] 2.1 (±0.1)[*]	0.9983[h] 0.9977[*]
Cromolyn	282 (±66)[h] 224 (±49)[*]	1 (±0.1)[h] 1 (±0.1)[*]	0.9898[h] 0.9862[*]
Taurocholate	– 273 (±18)[*]	– 2.3 (±0.2)[*]	– 0.9975[*]
Glycocholate	238 (±16)[h] 237 (±24)[*]	1.7 (±0.1)[h] 1.5 (±0.1)[*]	0.9983[h] 0.9958[*]
Allura red AC	6.0 (±0.3)[h] 15.5 (±1.4)[*]	2.2 (±0.2)[h] 2.3 (±0.2)[*]	0.9957[h] 0.9934[*]
Tartrazine	11.7 (±0.6)[h] 14.7 (±2.6)[*]	2.7 (±0.2)[h] 1.7 (±0.2)[*]	0.9978[h] 0.9912[*]
TNS	61.3 (±1.5)[h] 60.1 (±1.0)[*]	3.0 (±0.2)[h] 3.7 (±0.2)[*]	0.9982[h] 0.9978[*]

Table 1.

LL-37 binding parameters (K_d and the Hill coefficient) of folding inducer agents estimated from non-linear regression analysis of the changes of the helical content[h] (%) and the CD extremum[*] of the n-π^* band ($\Delta\Theta$ in mdeg measured between 222-226 nm). Experimental data were acquired in 10 mM Tris-HCl buffer at pH 7.4. No reliable fit could be obtained for the $\Delta\Theta$ values and the helical content of stercobilin and taurocholate, respectively.

Ligand	K_d (μM)	h	R^2
Olsalazine	26.7 (±1.4)	1.9 (±0.1)	0.9949
Balsalazide	160 (±25)	1.8 (±0.2)	0.9967
Diclofenac	97.3 (±12)	1.7 (±0.2)	0.9937
Meclofenamic acid	70.5 (±7.3)	1.3 (±0.1)	0.9931
Tartrazine	35.1 (±3.6)	2.0 (±0.1)	0.9985

Table 2.

LL-37 binding parameters of some folding inducers at physiological chloride level estimated from non-linear regression analysis of the increase of n-π^* CD band ($\Delta\Theta$ in mdeg measured between 222-224 nm). CD spectroscopic data were acquired in 10 mM Tris-HCl buffer containing 130 mM NaCl (pH 7.4).

Name	Q	A_S / Å^2	N^{c}_{total}	$\Delta\bar{G}_{bind}$ / (kcal/mol)	$\bar{K}_d^{calc}$ / μM	Clust. No.	f	$\Delta\bar{G}^{c}_{bind}$ / (kcal/ mol)
Olsalazine	-2	270.17±0.12	18	-5.20±0.02	176±6	1.	0.329	-5.28±0.03
						2.	0.328	-5.28±0.02
						3.	0.137	-5.30±0.03
Balsalazide	-2	337.55±0.19	34	-4.64±0.03	525±27	1.	0.313	-4.95±0.05
						2.	0.213	-4.45±0.04
						3.	0.133	-4.63±0.06
Sulfasalazine	-2	349.32±0.31	16	-4.59±0.04	495±16	1.	0.369	-4.83±0.03
						2.	0.310	-4.35±0.02
						3.	0.159	-4.60±0.04
Diclofenac	-1	255.37±0.07	16	-4.42±0.02	656±22	1.	0.530	-4.66±0.01
						2.	0.248	-4.22±0.01
						3.	0.049	-4.07±0.03
Meclofenamic acid	-1	259.33±0.04	11	-4.65±0.01	410±9	1.	0.886	-4.70±0.007
						2.	0.045	-4.26±0.01
						3.	0.033	-4.25±0.03
Ibuprofen	-1	240.00±0.15	11	-4.91±0.01	264±5	1.	0.395	-4.90±0.01
						2.	0.381	-4.98±0.02
						3.	0.084	-4.90±0.02
Glycocholate	-1	403.20±0.61	89	-4.41±0.05	1124±88	1.	0.091	-5.69±0.19
						2.	0.065	-4.53±0.10
						3.	0.064	-4.83±0.11
Tartrazine	-3	386.09±0.14	15	-5.27±0.03	194±10	1.	0.323	-5.75±0.03
						2.	0.186	-5.47±0.03
						3.	0.162	-5.09±0.02
TNS	-1	303.57±0.04	10	-4.22±0.01	829±11	1.	0.550	-4.23±0.01
						2.	0.192	-4.15±0.003
						3.	0.102	-4.25±0.02

Table 3.

Docking results of the selected molecules. Molecular properties (charge at pH 7.4 (Q), surface area (A_S), average binding free energies ($\Delta\bar{G}_{bind}$), average inhibitory constants ($\bar{K}_d^{calc}$) and results of clustering (total number of clusters (N^{c}_{total}), fraction of the clusters (*f*), binding free energy of the clusters $\Delta\bar{G}^{c}_{bind}$) are shown. The 95% confidence intervals was calculated using *t*-distribution.

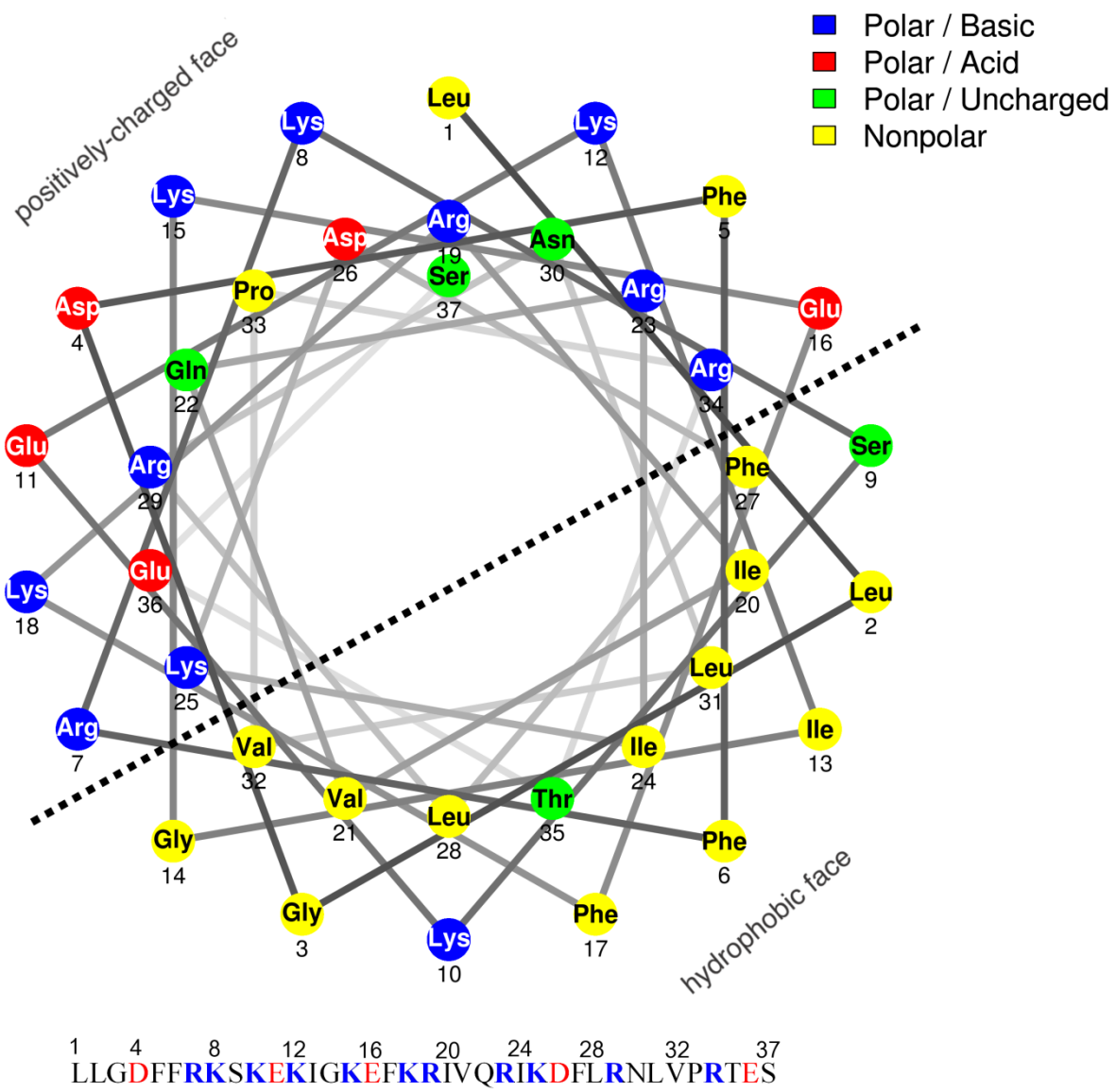

Scheme 1.

The amino acid sequence and helix-wheel representation of the human LL-37.

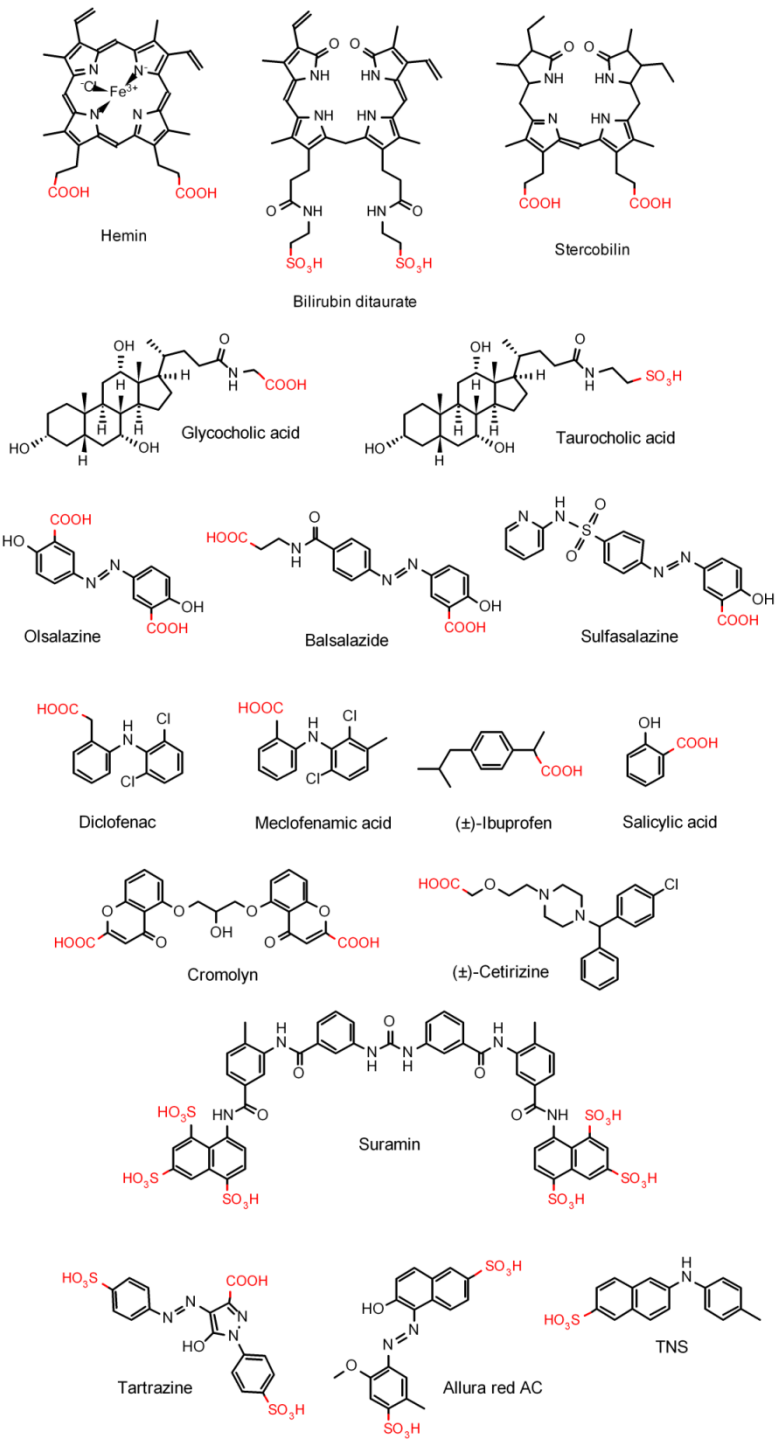

Scheme 2.

The chemical structure of small molecules used in this study.

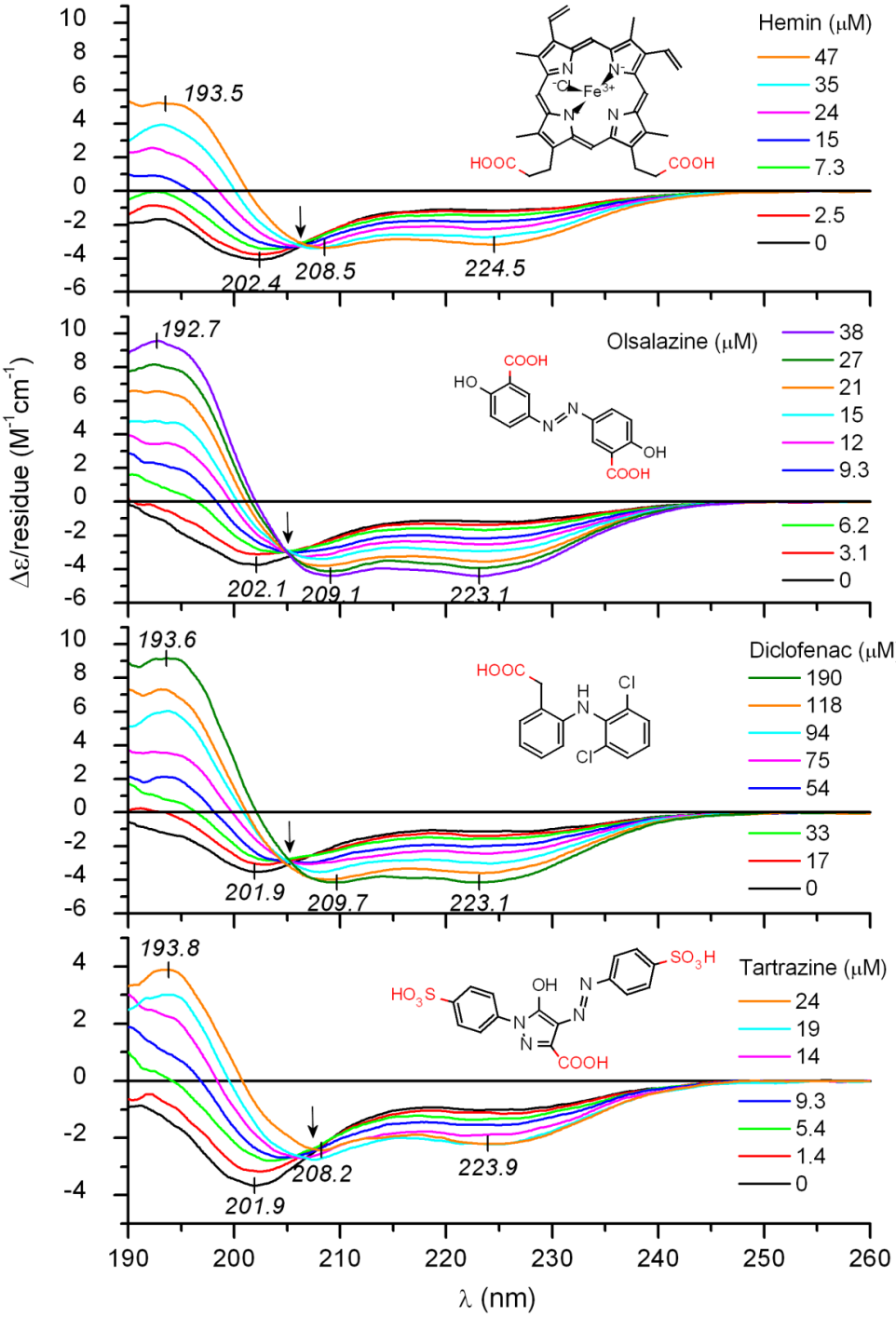

Figure 1. Representative far-UV CD spectroscopic changes of LL-37 (18 μM) measured upon consecutive addition of various organic compounds into the sample solution (10 mM Tris-HCl buffer at pH 7.4). Arrows denote isosbestic points around 205-207 nm.

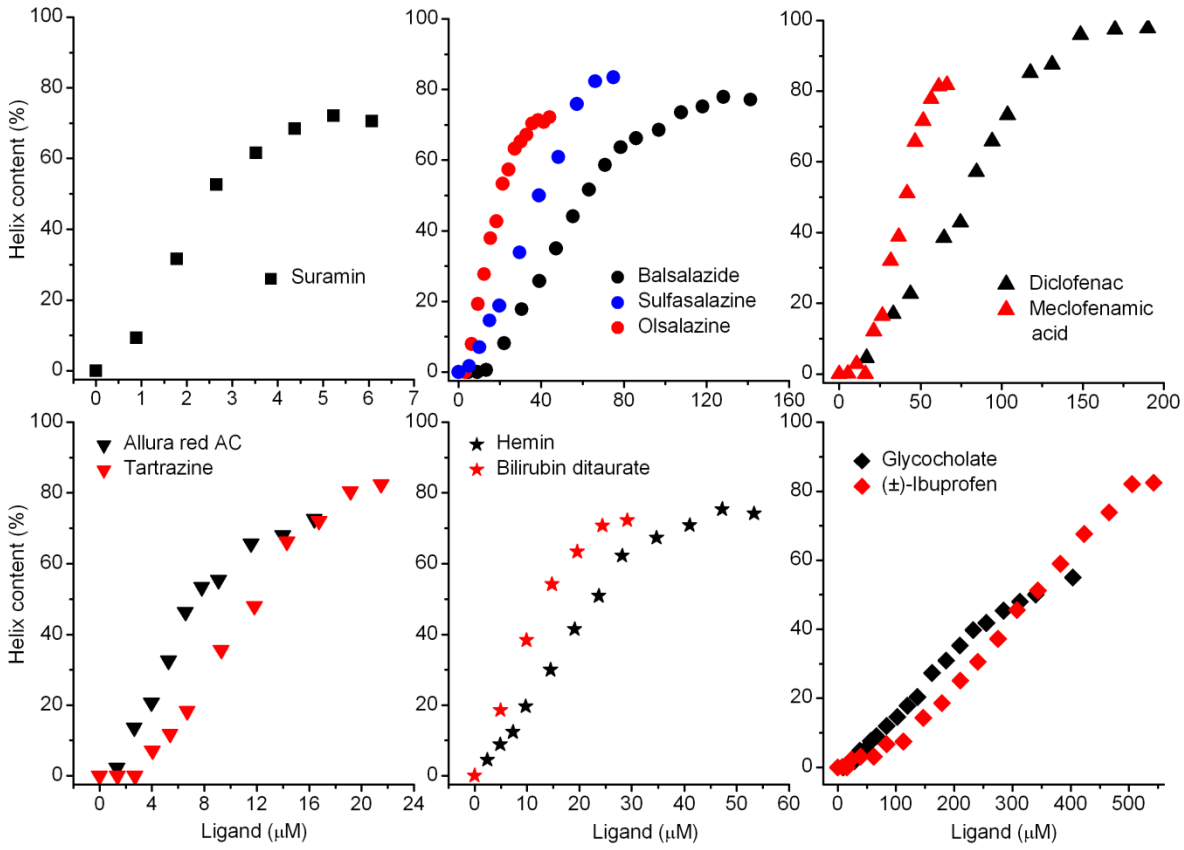

Figure 2.

Selected examples for changes of the helix content of LL-37 elicited by various small molecules.

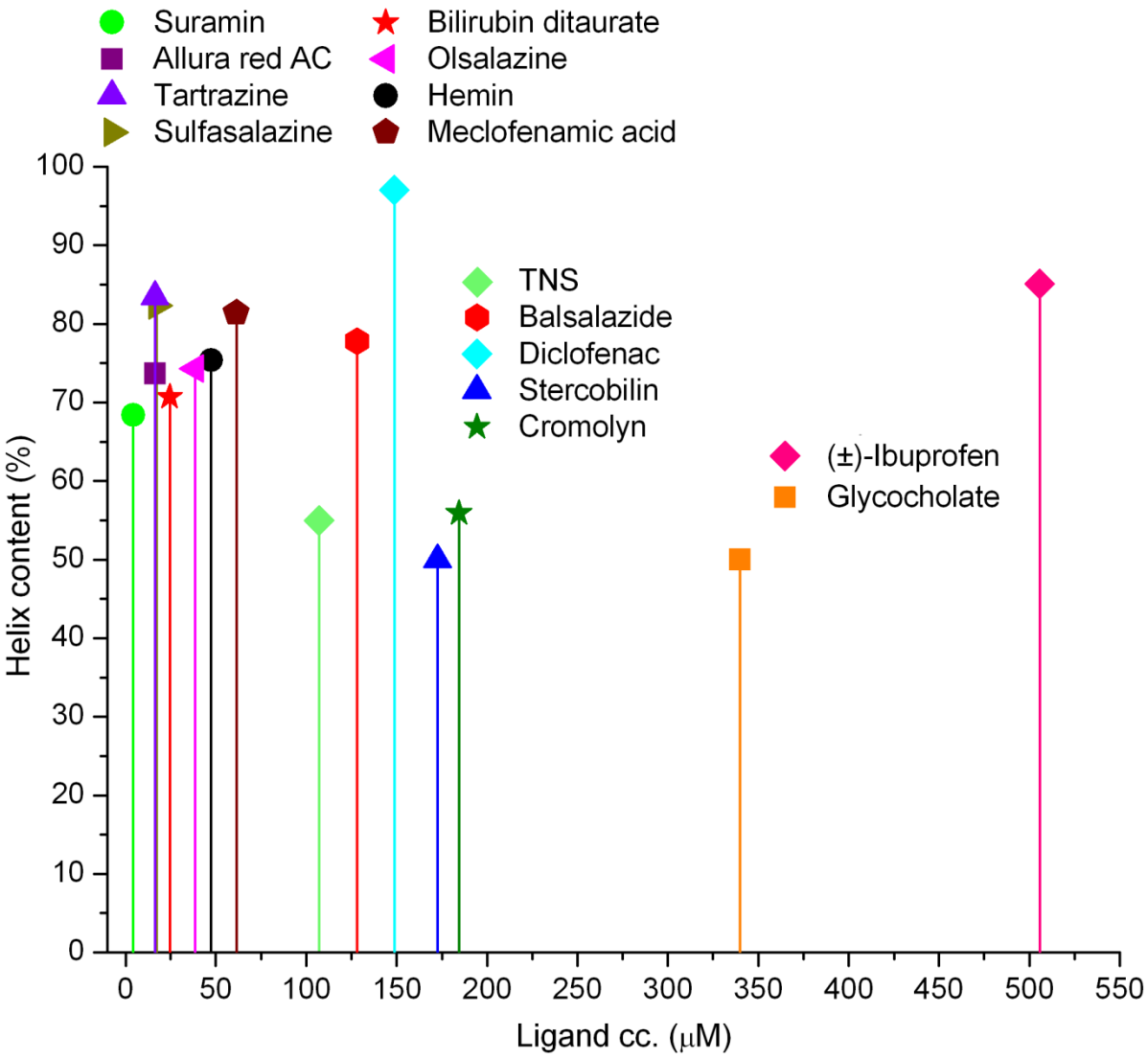

Figure 3.

Maximum helix content of LL-37 (18 μM) induced by a variety of small molecules.

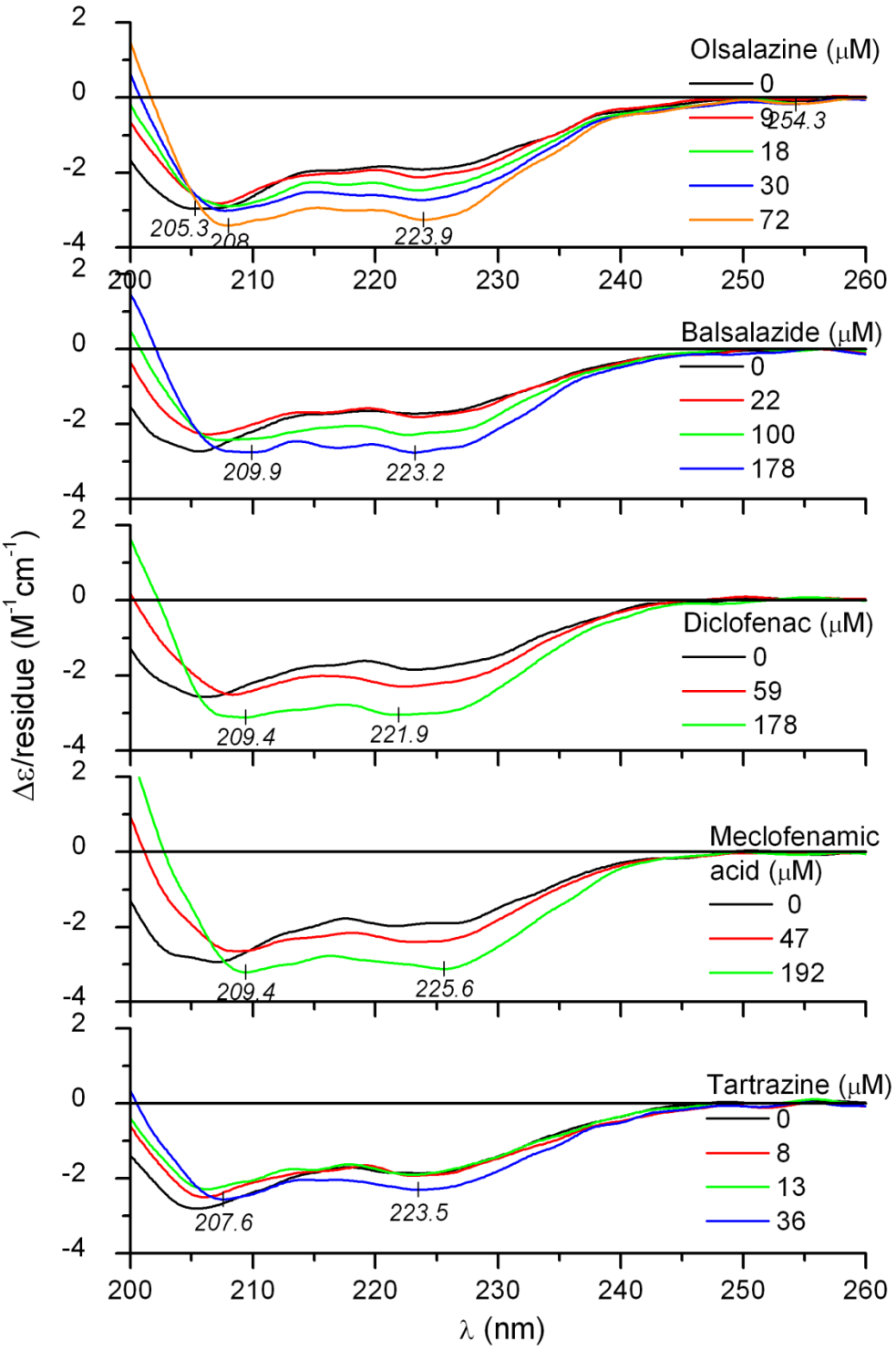

Figure 4.

Effect of small molecules on the far-UV CD spectrum of LL-37 (10 μM) measured in 10 mM Tris-HCl buffer containing 130 mM sodium chloride (pH 7.4).

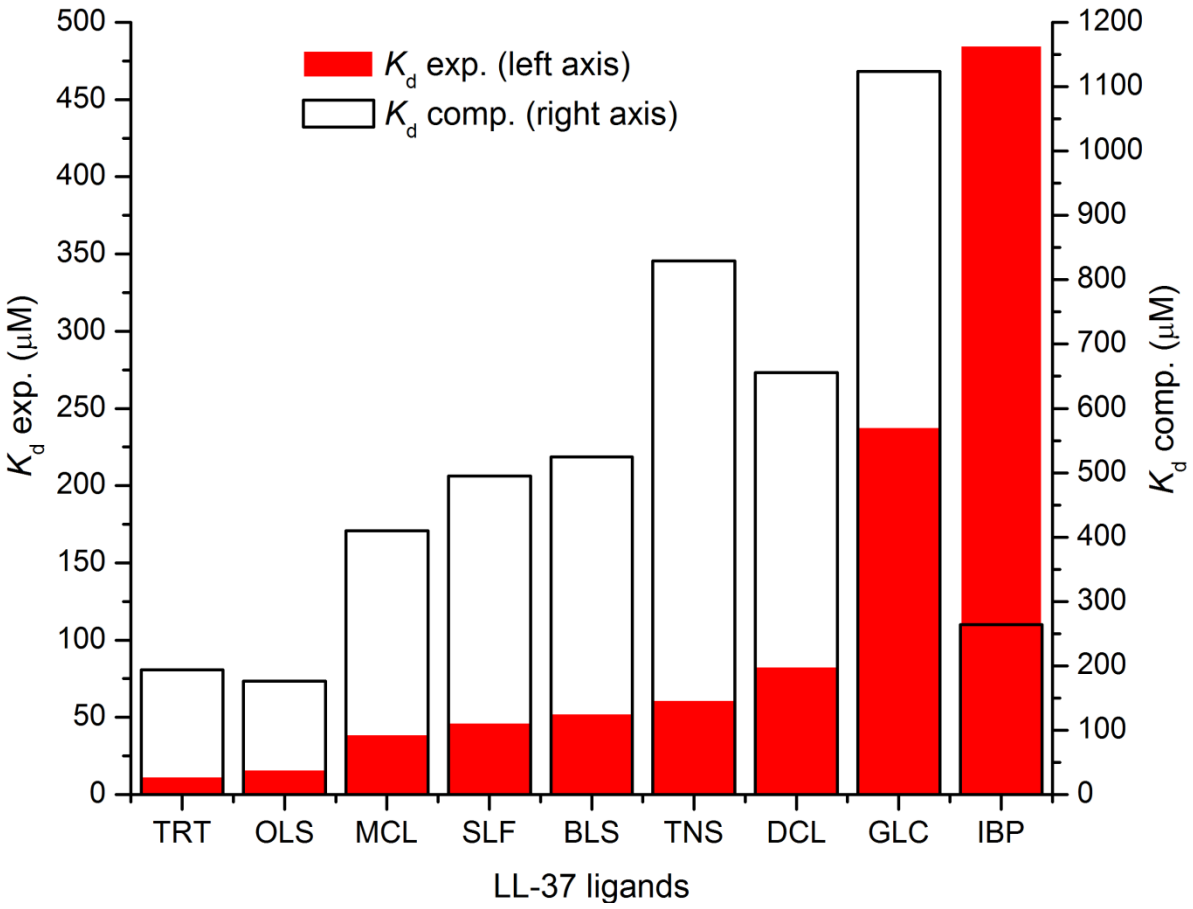

Figure 5.

Comparison of the experimental (Table 1, helical content) and computed (Table 3) K_d values of various ligands on LL-37. TRT: tartrazine; OLS: olsalazine; MCL: meclofenamic acid; SLF: sulfasalazine; BLS: balsalazide; TNS: 2-(*p*-toluidino)-6-naphthalenesulfonic acid; DCL: diclofenac; GLC: glycocholate; IBP: ibuprofen.

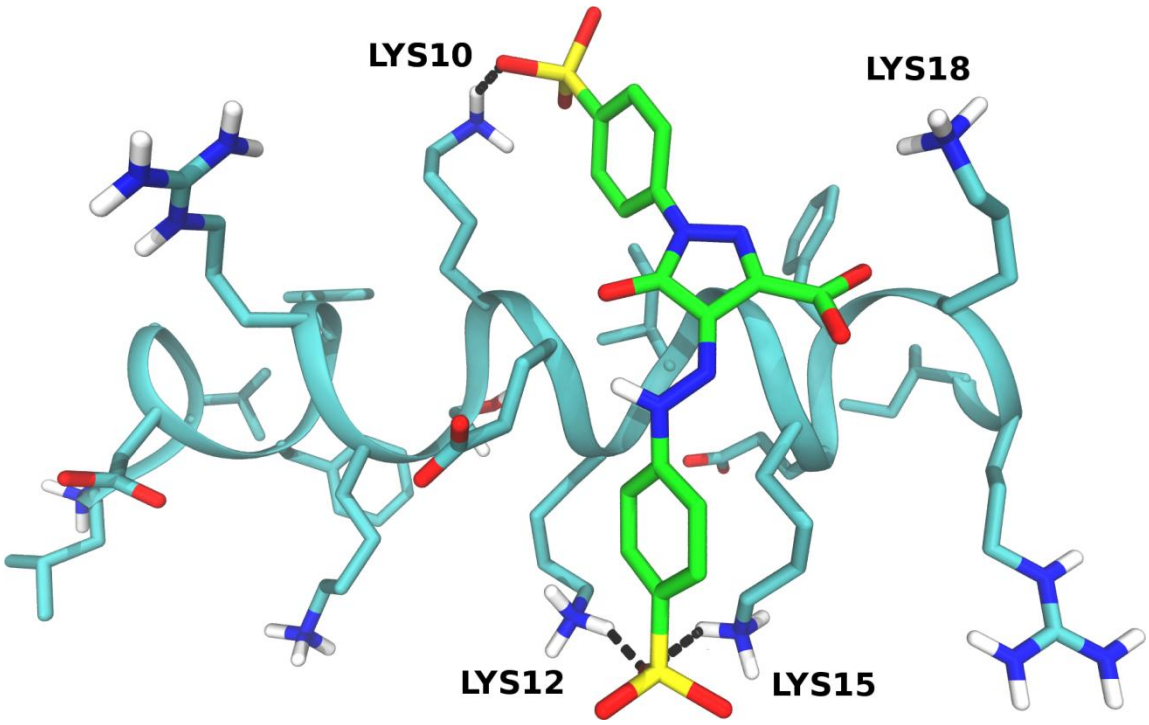

Figure 6.

Preferred binding site of tartrazine on LL-37. H atoms bonded to C atoms are not shown. Green: carbon (ligand); cyan: carbon (LL-37); white: hydrogen; blue: nitrogen; red: oxygen; yellow: sulfur. Dashed lines show ligand-residue salt bridges.

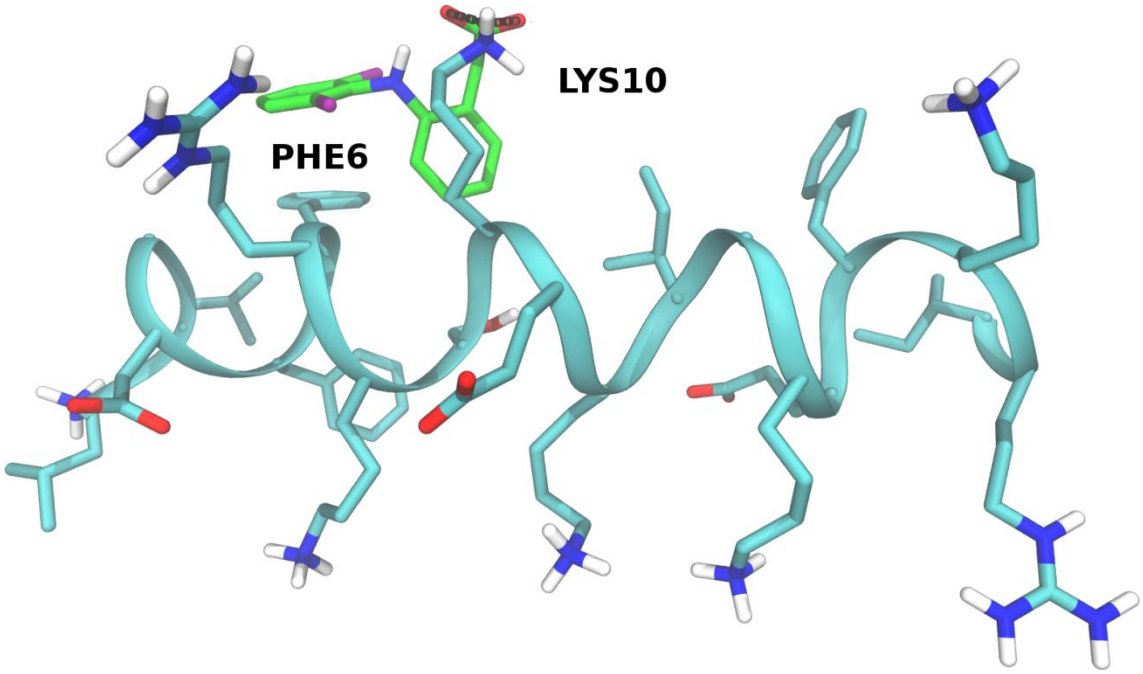

Figure 7.

Preferred binding site of diclofenac on LL-37. H atoms bonded to C atoms are not shown. Green: carbon (ligand); cyan: carbon (LL-37); white: hydrogen; blue: nitrogen; red: oxygen; yellow: sulfur. Dashed lines show salt bridges between Lys10 and the ligand molecule.

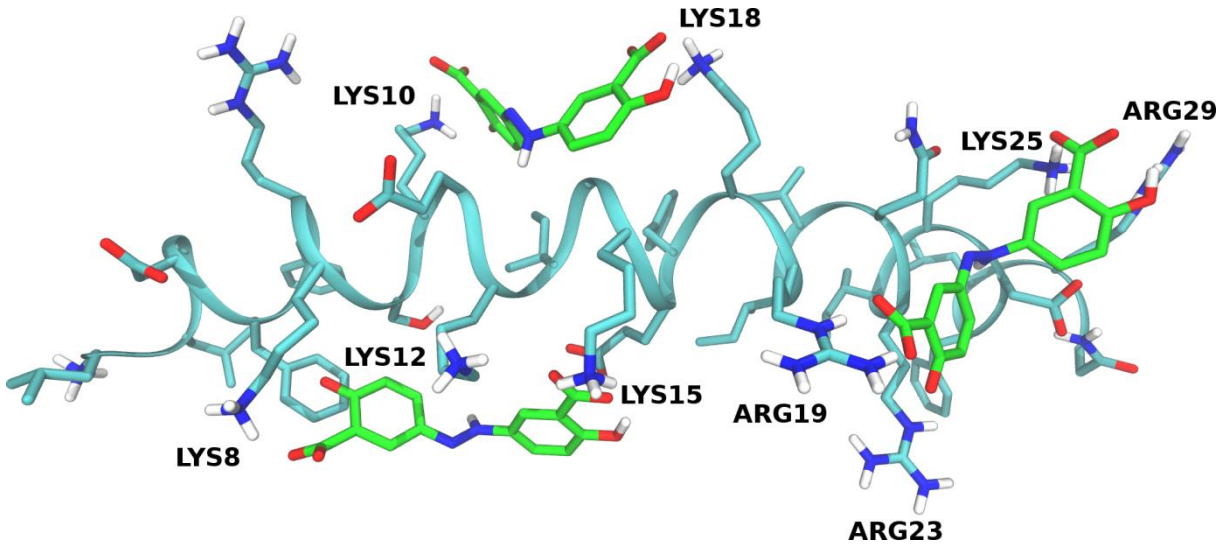

Figure 8.

A multiple binding mode of olsalazine molecules on LL-37 based on representatives of other clusters. H atoms bonded to C atoms are not shown. Green: carbon (ligand); cyan: carbon (LL-37); white: hydrogen; blue: nitrogen; red: oxygen; yellow: sulfur.

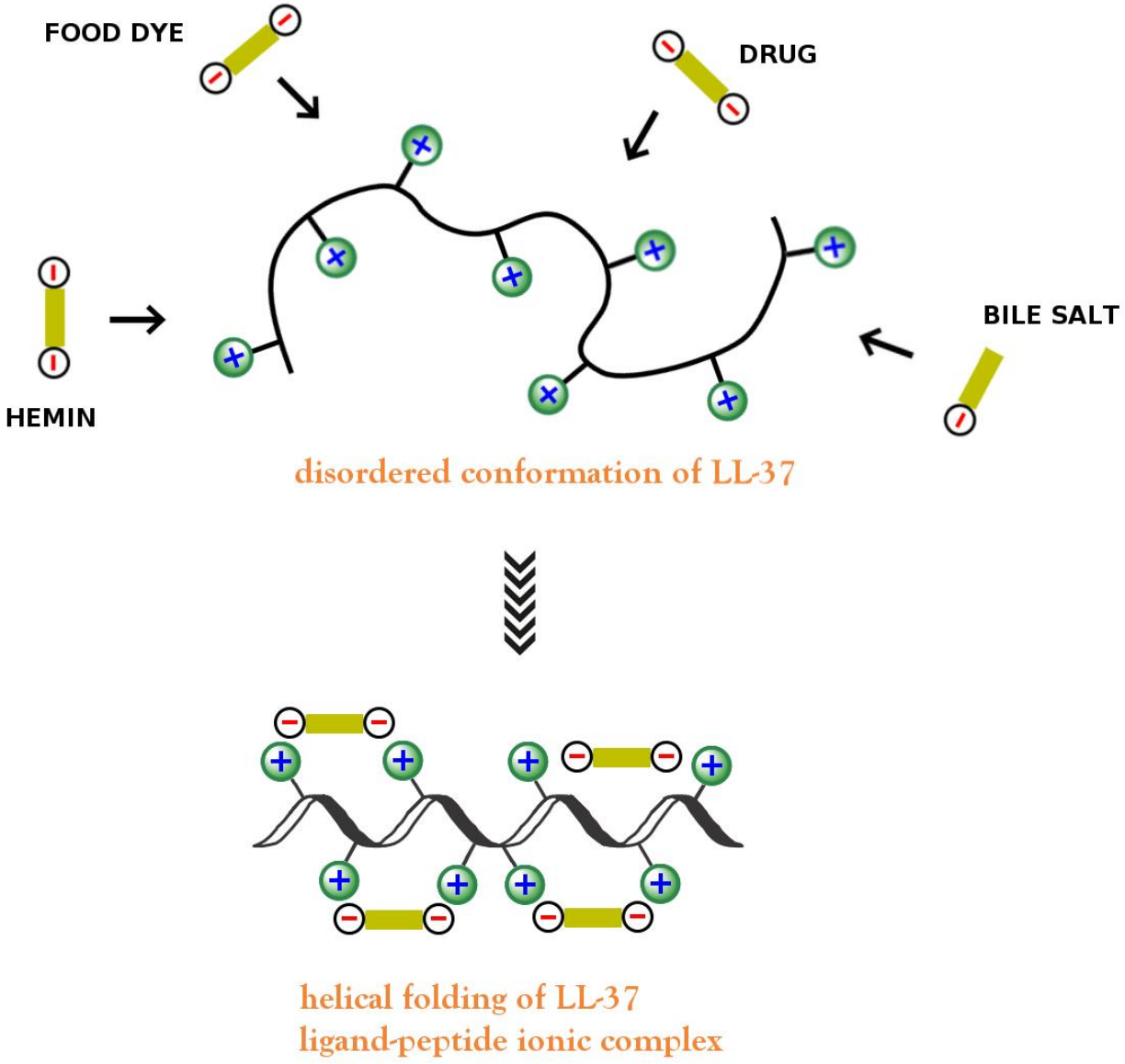

Graphical abstract

Highlights

- Ligand binding induced helical folding of the immunomodulatory and host-defense peptide LL-37 is demonstrated.
- Its rapid, disorder-to-order conformational conversion is provoked by chemically diverse, synthetic and natural organic compounds including antiinflammatory drugs, porphyrin pigments, bile salts and food dyes.
- Cooperative accommodation of the ligand molecules to the Lys8-Arg19 segment of the peptide results in multimeric complexes stabilized mainly by ionic interactions.
- These findings could be of interest both in drug pharmacology and to understand the pleiotropic biological functions of LL-37.

Supplementary Tables

	Surface area / Å^2	Total no. of clusters	Avg. energy / (kcal/mol)	K_d^{calc}/ μM	K_d^{exp1}/ μM	K_d^{exp2} / μM
Surface area / Å^2	1.00	0.48	0.15	0.27	-0.28	-0.27
Total number of clusters	0.48	1.00	0.05	0.18	0.03	-0.02
Avg. energy / (kcal/mol)	0.15	0.05	1.00	0.95	0.58	0.60
K_d^{calc}/ μM	0.27	0.18	0.95	1.00	0.62	0.60
K_d^{exp1}/ μM	-0.28	0.03	0.58	0.62	1.00	0.98
K_d^{exp2}/ μM	-0.27	-0.02	0.60	0.60	0.98	1.00

Table S1.

Correlation table of Spearman's correlation coefficients for experimental and calculated properties. Based on all docked molecules.

	Surface area / Å^2	Total no. of clusters	Avg. energy / (kcal/mol)	K_d^{calc}/ μM	K_d^{exp1}/ μM	K_d^{exp2}/ μM
Surface area / Å^2	1.00	0.37	0.02	0.19	0.02	0.05
Total number of clusters	0.37	1.00	0.01	0.17	0.32	0.26
Average energy / (kcal/mol)	0.02	0.01	1.00	0.93	0.90	0.93
K_d^{calc}/ μM	0.19	0.17	0.93	1.00	0.95	0.93
K_d^{exp1}/ μM	0.02	0.32	0.90	0.95	1.00	0.98
K_d^{exp2}/ μM	0.05	0.26	0.93	0.93	0.98	1.00

Table S2.

Correlation table of Spearman's correlation coefficients for experimental and calculated properties. Based on the docked molecules excluding ibuprofen.

Supplementary Figures

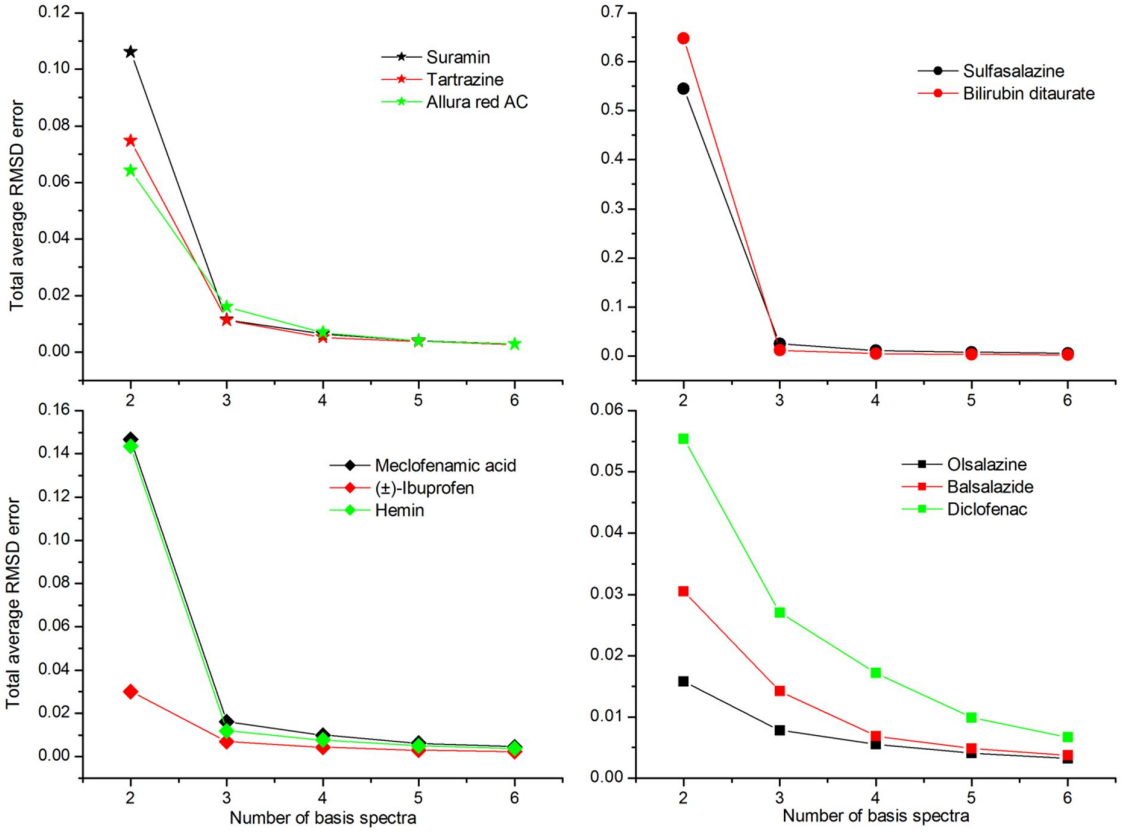

Figure S1.

The dependence of total average RMSD values on the numbers of pure CD components obtained by the CCA+ analysis.

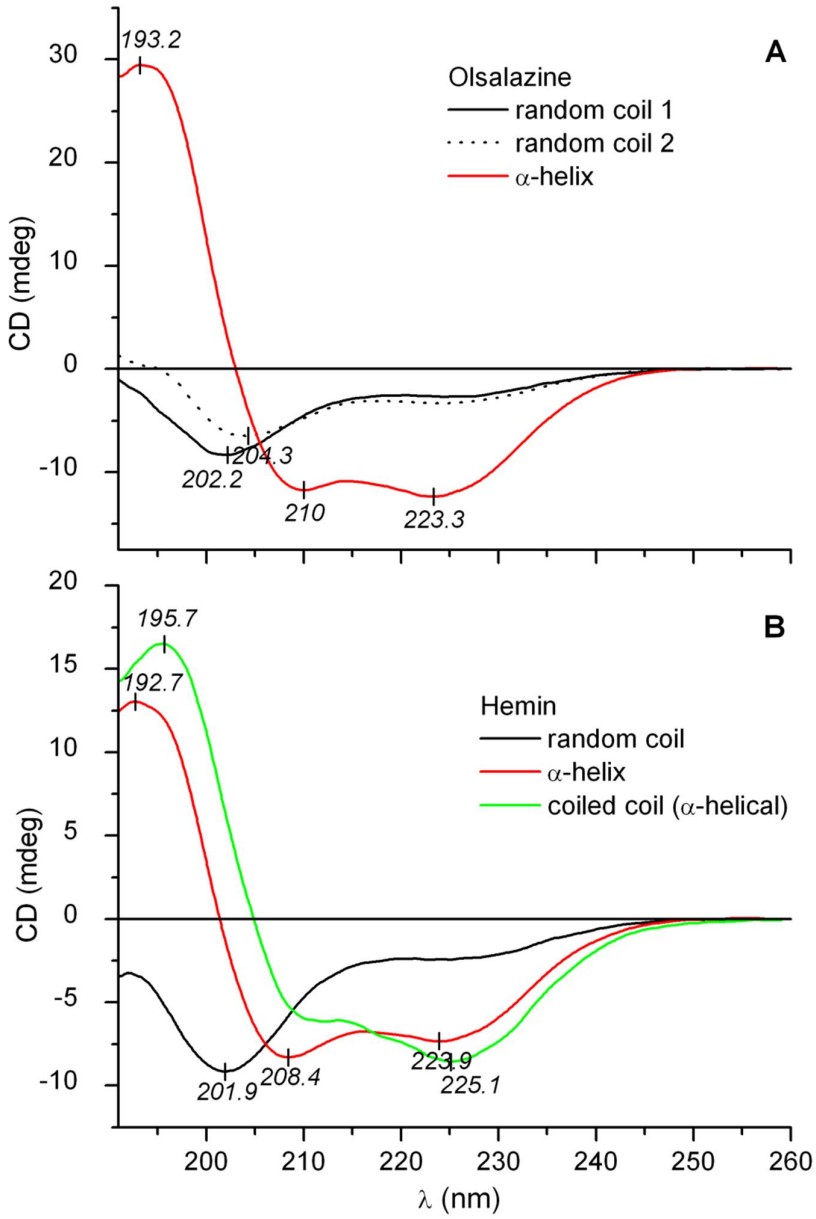

Figure S2.

Two types of the pure-component CD spectra sets as a result of the CCA+ analysis of CD titration curves of LL-37.

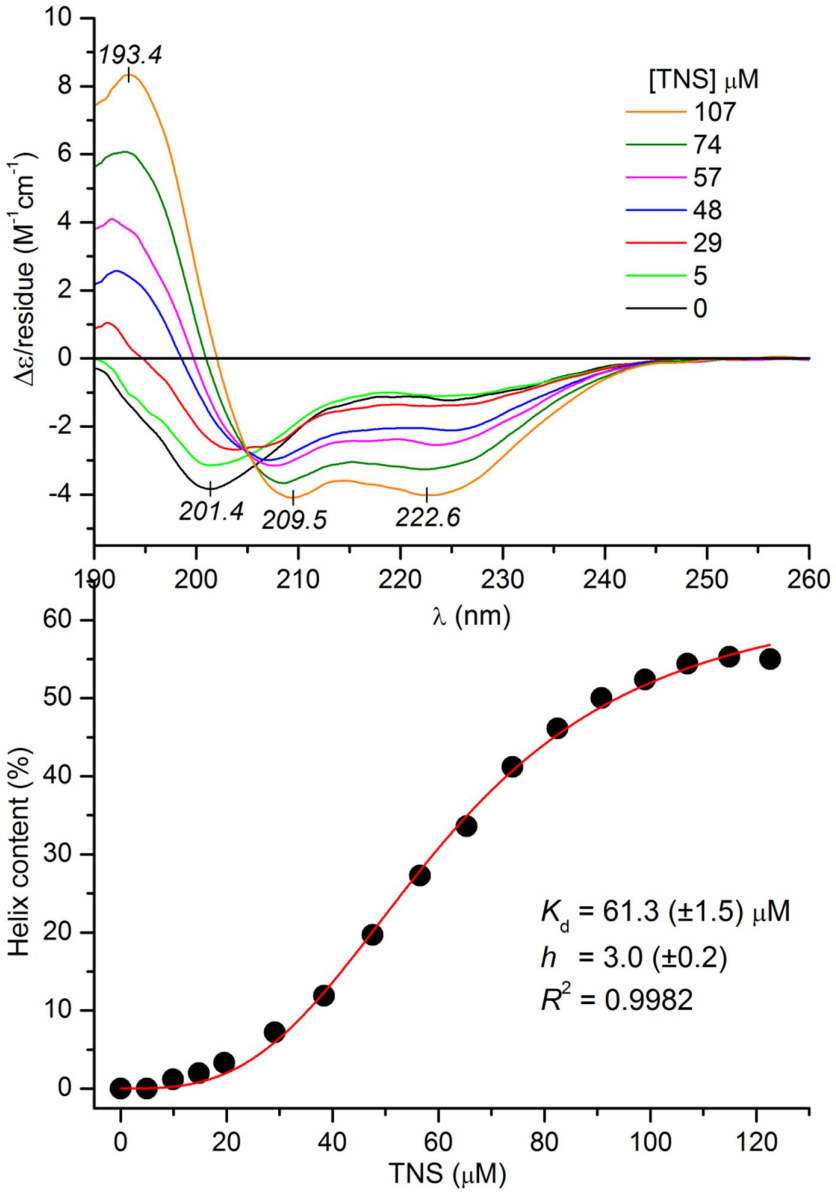

Figure S3.

Top panel: selected far-UV CD spectra of 18 μM LL-37 measured upon consecutive increase of TNS concentration in the sample solution (10 mM Tris-HCl buffer at pH 7.4).

Bottom panel: helix contents obtained from the CD titration data. Solid line is the result of non-linear curve fitting analysis performed by using the "One site - specific binding with Hill slope" equation built in the Graph Pad Prism software (ver. 6.01, San Diego, California, USA). K_d value and the Hill coefficient (h) are shown.

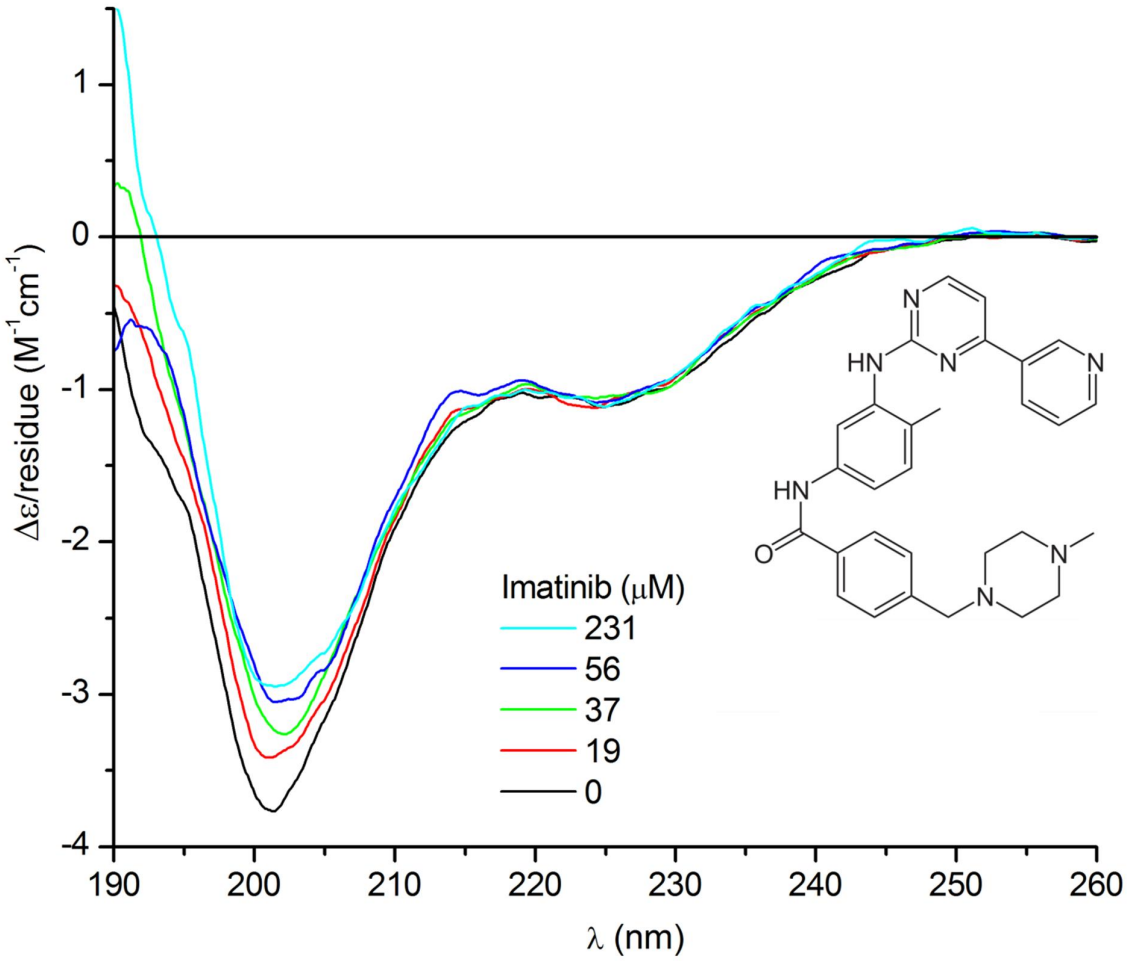

Figure S4.

Effect of imatinib on the far-UV CD spectrum of 18 μM LL-37 (10 mM Tris-HCl buffer at pH 7.4).

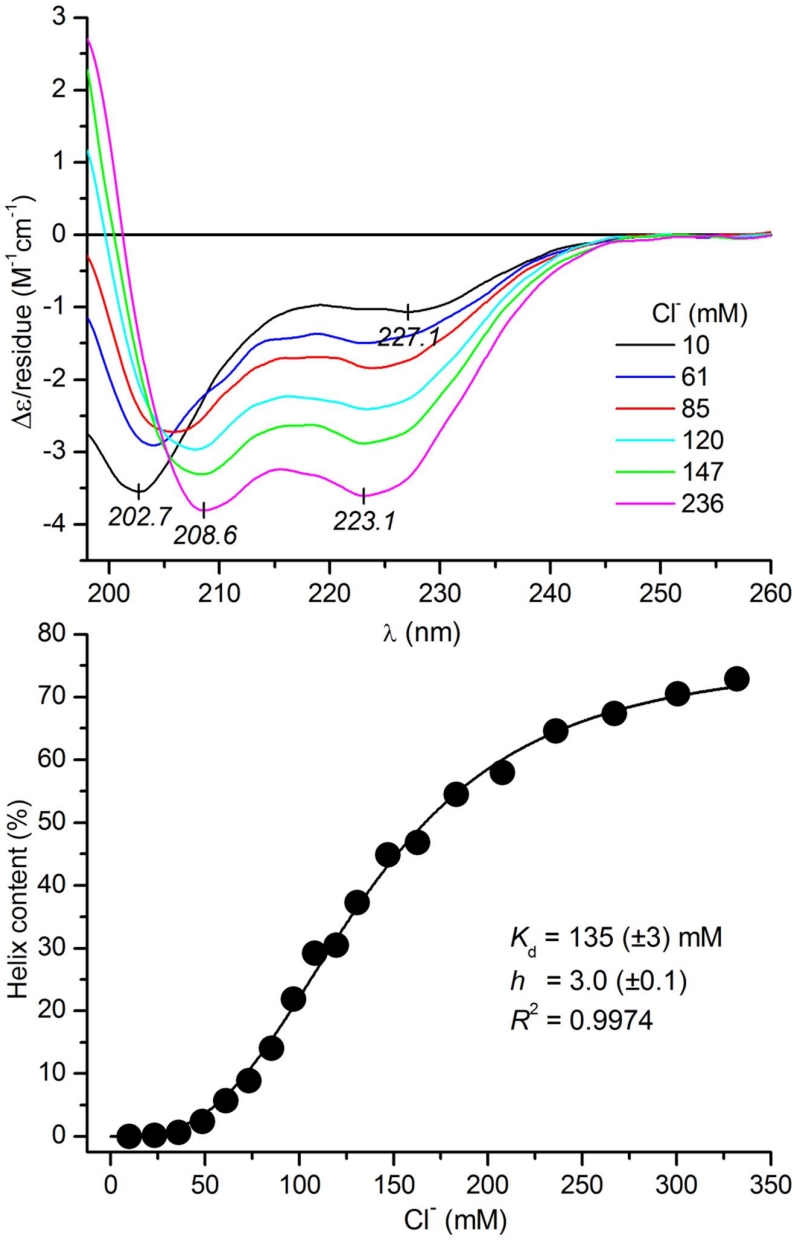

Figure S5.

Top panel: selected far-UV CD spectra of 18 μM LL-37 measured upon consecutive increase of sodium chloride concentration of the sample solution (10 mM Tris-HCl buffer at pH 7.4). Bottom panel: helix contents obtained from the CD titration data. Solid line is the result of non-linear curve fitting analysis performed by using the "One site - specific binding with Hill slope" equation built in the Graph Pad Prism software (ver. 6.01, San Diego, California, USA). K_d value and the Hill coefficient (h) are shown.

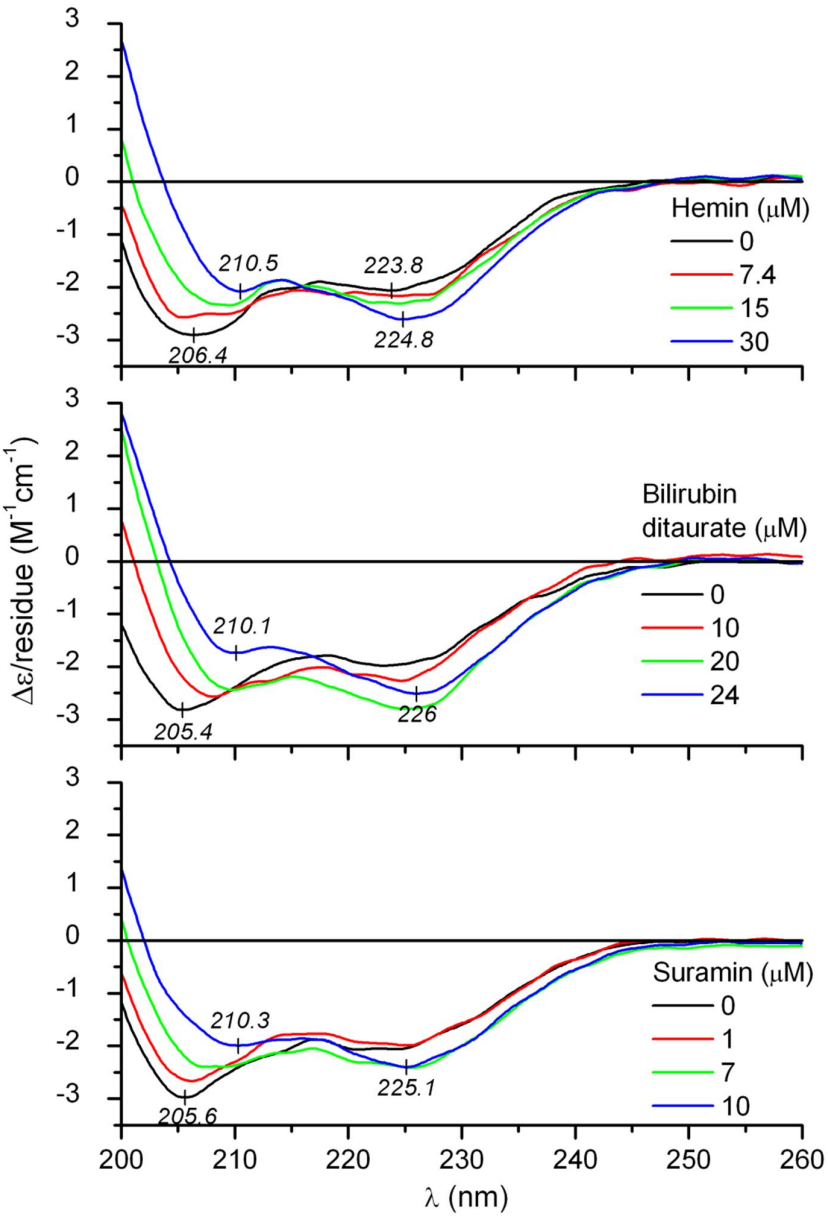

Figure S6.

Effect of porphyrin pigments and suramin on the far-UV CD spectrum of LL-37 (10 μM) measured in 10 mM Tris-HCl buffer containing 130 mM sodium chloride (pH 7.4).

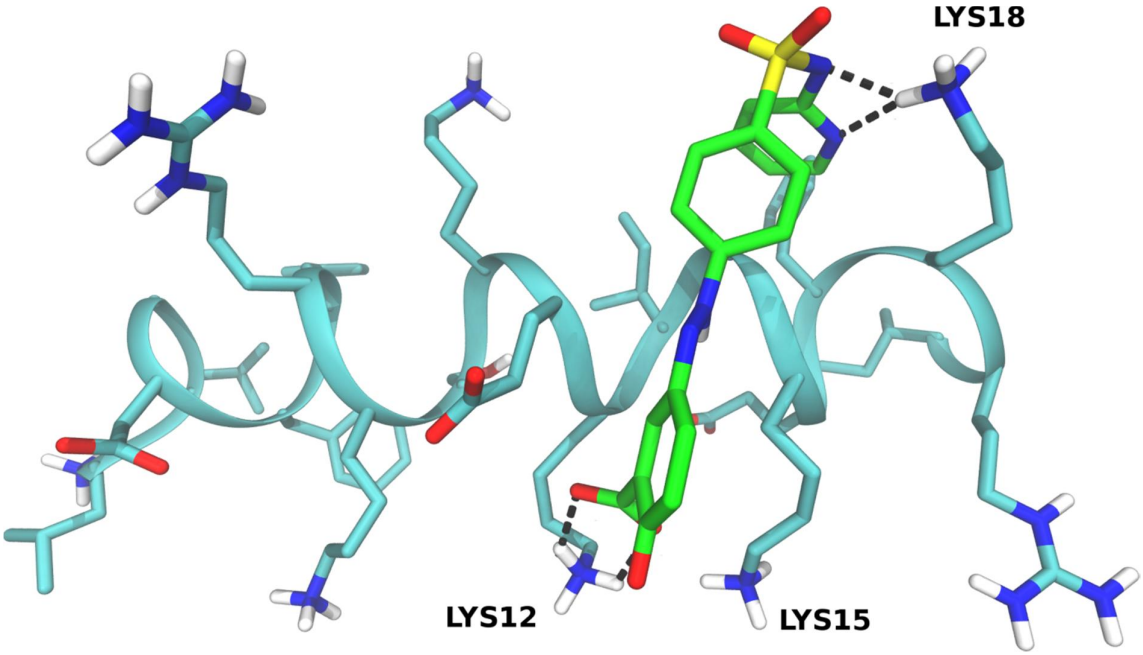

Figure S7.

The preferred binding site of sulfasalazine on LL-37. H atoms bonded to C atoms are not shown. Green: carbon (ligand); cyan: carbon (LL-37); white: hydrogen; blue: nitrogen; red: oxygen; yellow: sulfur. Dashed lines show ligand-residue salt bridges and two H-bonds with Lys18.

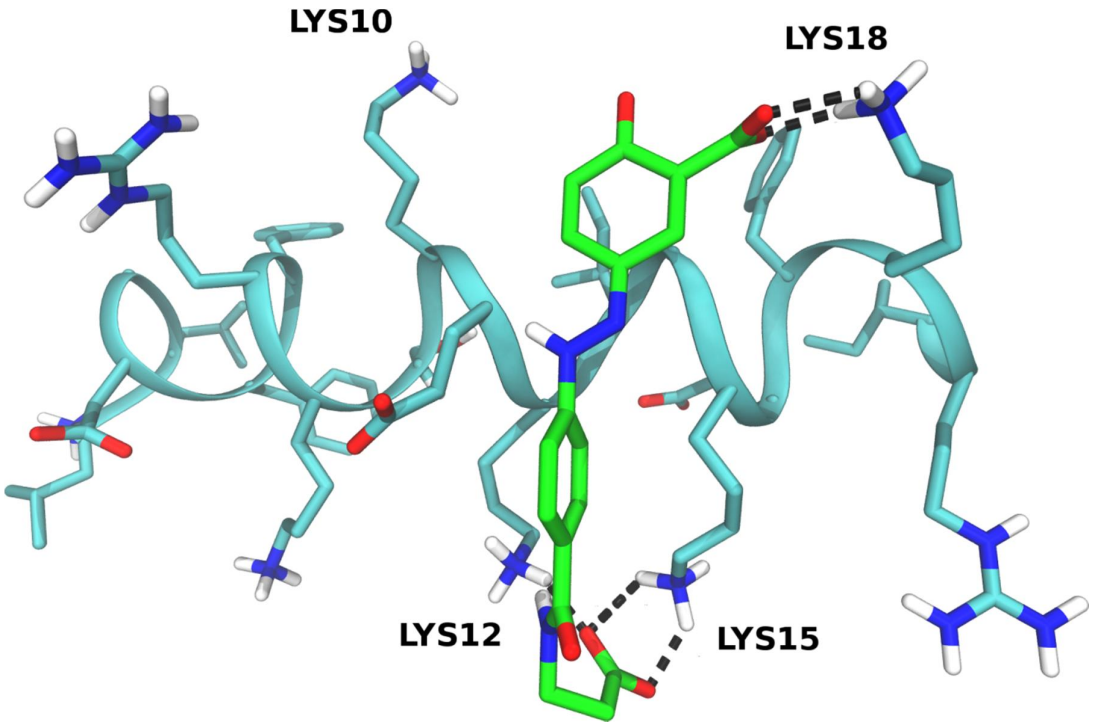

Figure S8.

The preferred binding site of balsalazide on LL-37. H atoms bonded to C atoms are not shown. Green: carbon (ligand); cyan: carbon (LL-37); white: hydrogen; blue: nitrogen; red: oxygen; yellow: sulfur. Dashed lines show ligand-residue salt bridges.

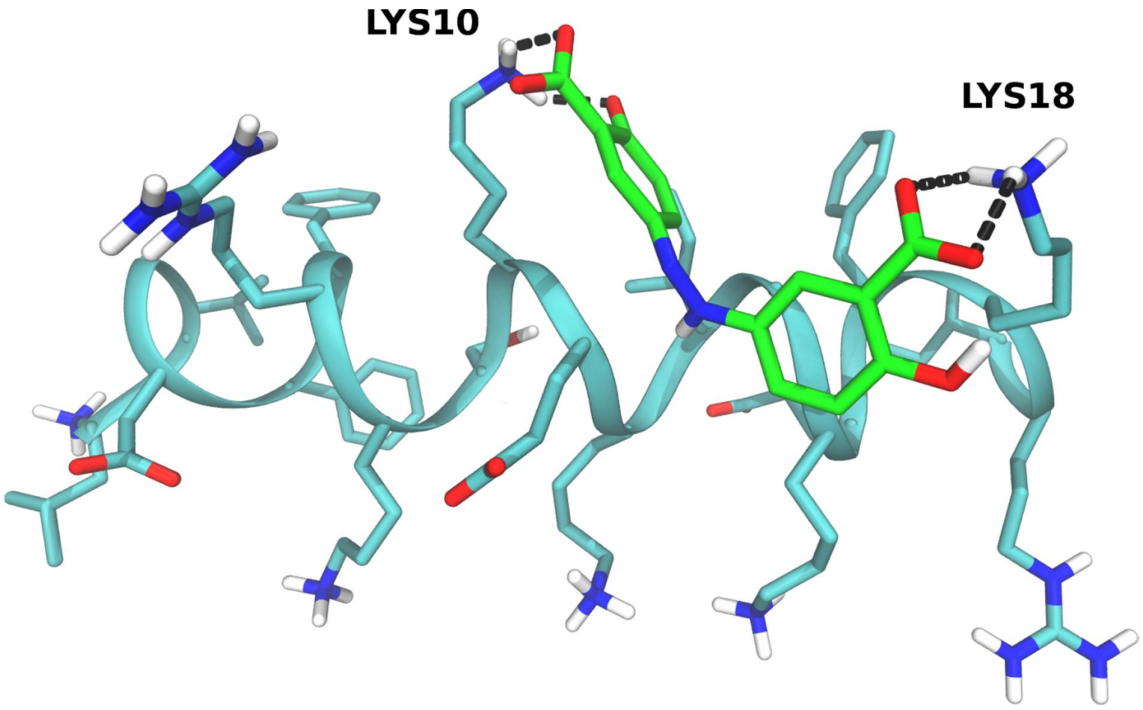

Figure S9.

The preferred binding site of olsalazine on LL-37. H atoms bonded to C atoms are not shown. Green: carbon (ligand); cyan: carbon (LL-37); white: hydrogen; blue: nitrogen; red: oxygen; yellow: sulfur. Dashed lines show ligand-residue salt bridges and H-bonds (Lys10---OH–).

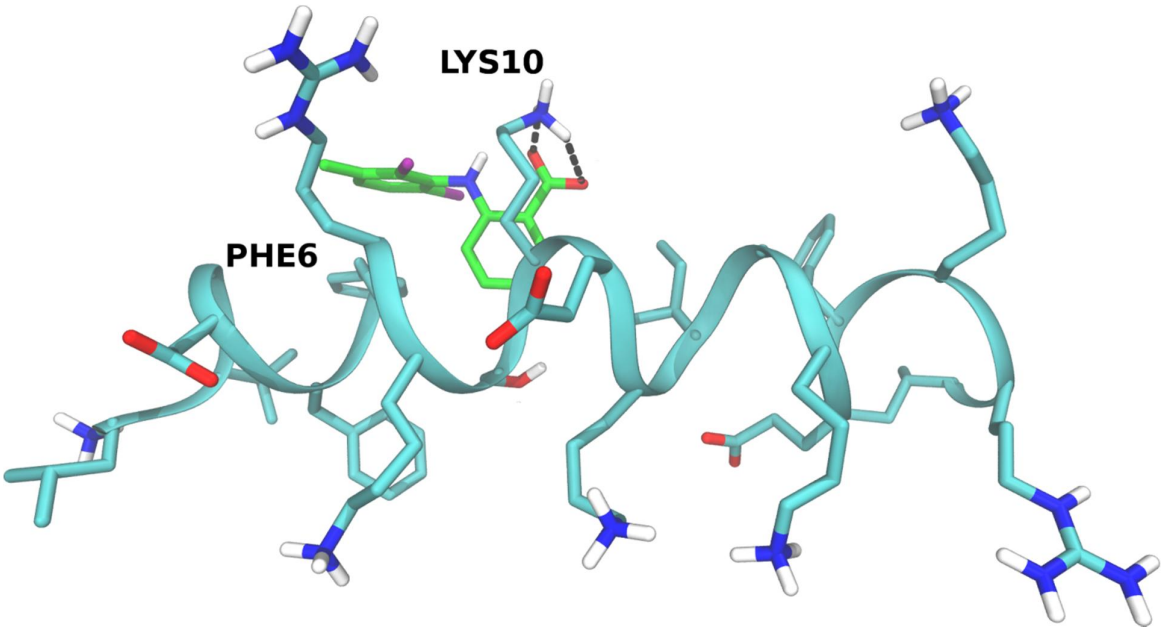

Figure S10.

The preferred binding site of meclofenamic acid on LL-37. H atoms bonded to C atoms are not shown. Green: carbon (ligand); cyan: carbon (LL-37); white: hydrogen; blue: nitrogen; red: oxygen; yellow: sulfur. Dashed lines show ligand-residue salt bridges.

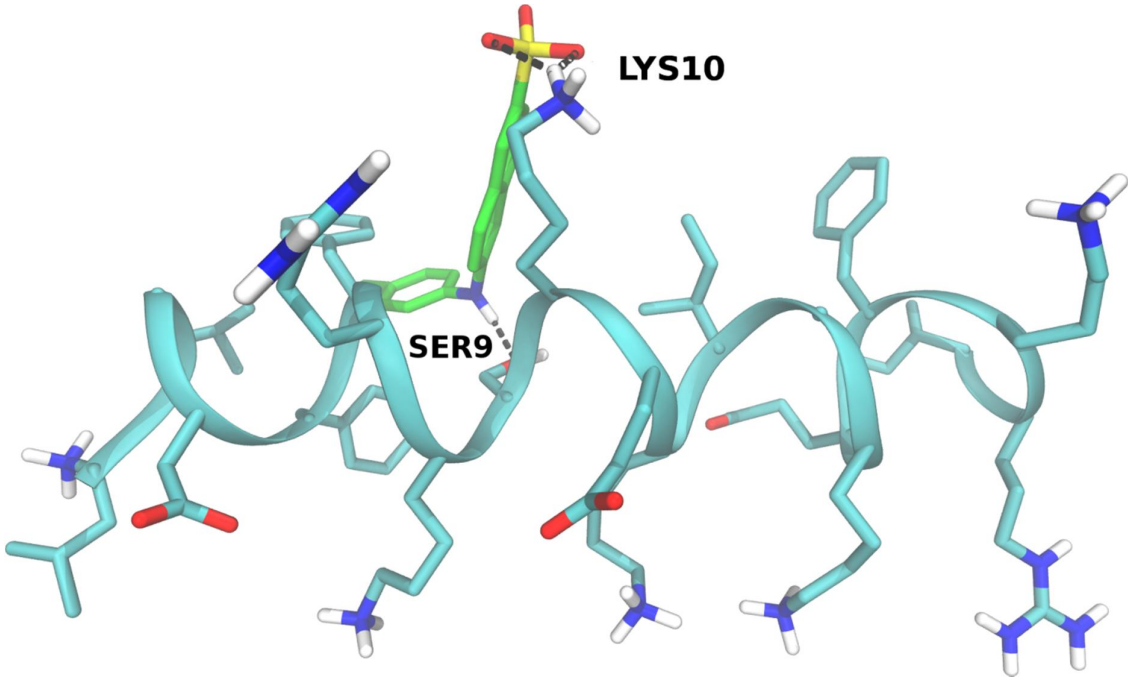

Figure S11.

The preferred binding site of TNS on LL-37. H atoms bonded to C atoms are not shown. Green: carbon (ligand); cyan: carbon (LL-37); white: hydrogen; blue: nitrogen; red: oxygen; yellow: sulfur. Dashed lines show ligand-residue salt bridges and H-bonds (Ser9---HN<).

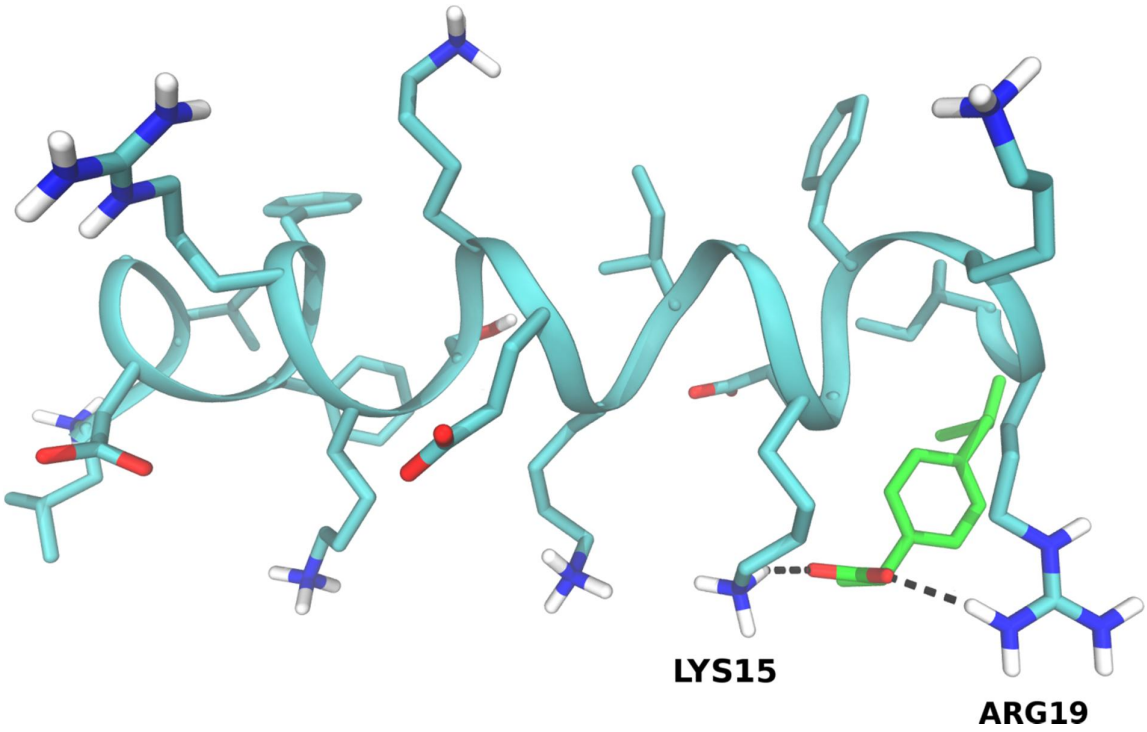

Figure S12.

The preferred binding site of *S*-ibuprofen on LL-37. H atoms bonded to C atoms are not shown. Green: carbon (ligand); cyan: carbon (LL-37); white: hydrogen; blue: nitrogen; red: oxygen; yellow: sulfur. Dashed lines show ligand-residue salt bridges.

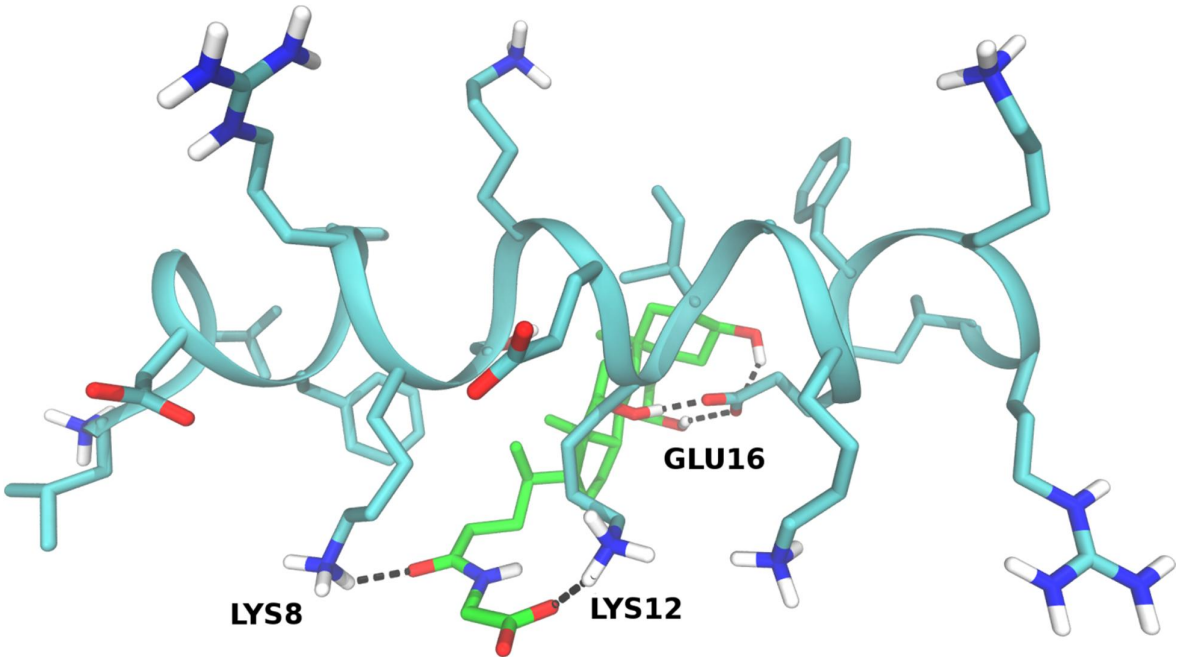

Figure S13.

The preferred binding site of glycocholic acid on LL-37. H atoms bonded to C atoms are not shown. Green: carbon (ligand); cyan: carbon (LL-37); white: hydrogen; blue: nitrogen; red: oxygen; yellow: sulfur. Dashed lines show ligand-residue salt bridges and H-bonds.

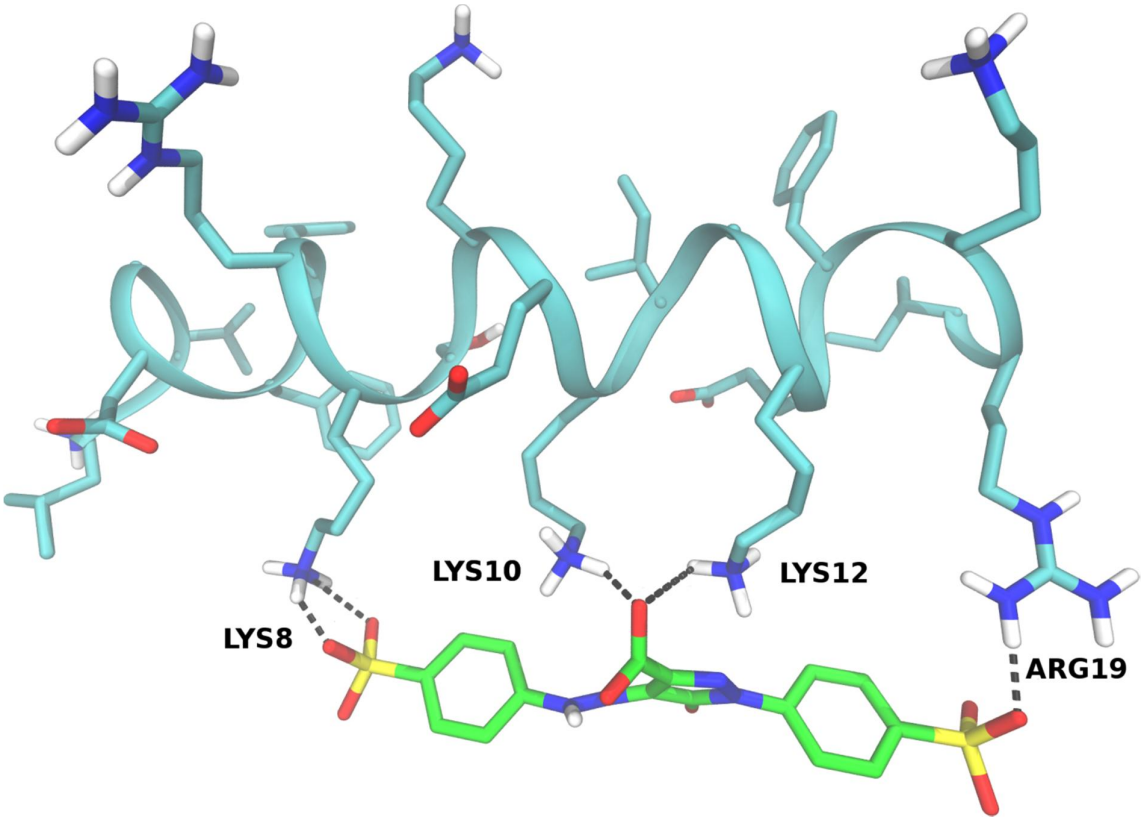

Figure S14.

The binding site of tartrazine on LL-37 based on cluster 3 (see Table 3 in the main text). H atoms bonded to C atoms are not shown. Green: carbon (ligand); cyan: carbon (LL-37); white: hydrogen; blue: nitrogen; red: oxygen; yellow: sulfur. Dashed lines show ligand-residue salt bridges.